Temperature dependence of a phytoplankton population in a 2D model of a coastal area

Barber Vos (5048826)

Bachelor End Project
BSc Applied Mathematics and
Applied Physics
Faculty of Electrical Engineering,
Mathematics and Computer Science
(EEMCS) and Applied Sciences (AS)
Delft University of Technology

Delft, June 12, 2022
Supervisors:
Dr. ir. Y.M. Dijkstra,
Prof. dr. ir. C.R. Kleijn

Abstract

Due to climate change, the sea temperature is rising. This temperature change has an effect on the phytoplankton population. Phytoplankton is responsible for more than 50 percent of the oxygen production on earth, and is therefore crucial for life on earth. In this report, the research question is: is the temperature increase of the water important for the development in space and time of the plankton population in a 2D model of a coastal area of an ocean?

To investigate this, first a 2D model for a coastal area of an ocean is formed. As a basis for this model the 0D model of Steele and Henderson is used to describe the predator-prey model for zooplankton and phytoplankton. Due to this model a repeating pattern in time arises, which is called a limit cycle. This predator-prey model is expanded to a 2D model by applying convection (v) and diffusion (D) to it, representing the current and dispersion in the water. The chosen parameters and boundary conditions are inspired by the coastal area of the west coast of Portugal.

To evaluate the effect of the water temperature rising, first, the effect of diffusion and convection are studied by answering the following questions: is the convection important for the development in space and time of the plankton population in a 2D model of a coastal area of an ocean? And: is the diffusion important for the development in space and time of the plankton population in a 2D model of a coastal area of an ocean?

The diffusion is dominant in the direction perpendicular to the coast. Due to the diffusion the limit cycle of the predator-prey model is suppressed. Its range gets smaller until the plankton population is completely constant for $D > 2.5$ m^2/s. This critical value is included in the realistic value of D, which varies from 1 to 2000 m^2/s.

Due to convection, the limit cycle corresponding to the boundary condition occurs in the direction parallel to the coast, making every point in the domain steady state. The higher the velocity v corresponding to the convection is, the less oscillations in phytoplankton density there are in the domain, thus the larger the wavelength of the oscillation is. For $v > 0.06$ m/s the current is so fast that the predator-prey model has little time to develop before it reaches the right boundary, making the left boundary value more important. This critical value is included in the realistic value of v, which varies from 0.03 to 0.28 m/s.

The model experiences both diffusion and convection more or less equally when the Péclet number $\frac{vH^2}{DL} \approx 1$, resulting in $\frac{D}{v} \approx 50$ m. If this number is significantly larger than 50 m, diffusion dominates the solution. If the number is significantly smaller than 50 m, convection dominates the solution.

Now the main research question can be answered. By increasing the temperature of the water the growth rate of phytoplankton increases. Due to this increase, the timescale of the predator-prey (τ_{pp}) decreases. The value of D and v for which the predator-prey model and diffusion and convection all influence the solution equally depends on the timescale with the factor $1/\tau_{pp}$. A smaller time scale means that the predator-prey model contributes more to the model. However, this change is very small in comparison to the scale of the realistic values. In conclusion, in the formed 2D model the temperature increase of the water is not important for the development of the plankton population in space and time.

The results of this report are influenced by the assumptions and approximations made. In this study, several processes, both physical and biological, are described with constants and simplifications. Improving the models of these processes is left for further research.

Table of Contents

1 Introduction

Plankton, and specifically phytoplankton, is responsible for more than 50 percent of the oxygen production on earth [22]. This is way more than the contribution of the rain forests. Not only does plankton produce oxygen, it also stores carbon dioxide [25]. In the current climate crisis, where too much carbon dioxide is released by humans, this is highly needed. Furthermore, phytoplankton forms the base of aquatic food webs [21]. Small fish and zooplankton eat phytoplankton. These animals themselves are eaten by bigger fish. Thus, the oceanic ecosystem is dependent on phytoplankton. In short, plankton is crucial for life on earth. However, plankton is often overlooked, and does not get as much appreciation as it should. As plankton is so crucial, the development of its population should be studied.

Plankton comes from the Greek word '$\pi\lambda\alpha\gamma\tau o\varsigma$ ', which means drifter [20]. An organism is called plankton if it is carried by currents and tides, and cannot move against these forces. Plankton can be divided into two groups: phytoplankton and zooplankton. Phytoplankton consists of microscopic plants which perform photosynthesis. As the phytoplankton needs sunlight to perform photosynthesis, it is found near the surface of the water. Zooplankton consists of microscopic animals which eat phytoplankton.

The current research on mathematical models to describe the development of a plankton population is limited. Steele and Henderson have created a 0D model of coupled ordinary differential equations to describe the predator-prey model for zooplankton and phytoplankton [26]. There is a knowledge gap in expanding this model to a depth integrated 2D model in which physical transport is considered [2]. To do this a numerical model should be formed.

Furthermore, the temperature dependence on the growth term of phytoplankton is known, but the effect of it in a 2D model is not. In this report, the research question is: is the temperature increase of the water important for the development in space and time of the plankton population in a 2D model of a coastal area of an ocean?

To investigate this, first a 2D model for a coastal area of an ocean is formed. As a basis for this model the 0D model of Steele and Henderson is used to describe the predator-prey model for zooplankton and phytoplankton [26]. This model has no spatial dimensions and is expanded to a 2D model by applying convection and diffusion to it, representing the current and dispersion in the water. The chosen parameters and boundary conditions are inspired by the coastal area of the west coast of Portugal.

To understand the effect of temperature change on this model, first the three mechanisms (convection, diffusion and the predator-prey model) in the 2D model and their contribution have to be understood. Therefore the following sub questions arise: Is the convection important for the development in space and time of the plankton population in a 2D model of a coastal area of an ocean? And is the diffusion important for the development in space and time of the plankton population in a 2D model of a coastal area of an ocean?

To answer these questions, first in chapter 2 the 0D model of Steele and Henderson is explained and analysed. Next, in chapter 3 the model is expanded to a 2D model using convection and diffusion. In addition, this model and its separate mechanisms are analysed. Lastly, in chapter 4 the effect of temperature change of the water is studied. In chapter 5 the used approximations and found results are discussed, and in chapter 6 the conclusion is formed.

2

Steele and Henderson Model

In 'The role of predation in plankton models' written by John H. Steele and Eric W. Henderson a simple predator-prey model is described to analyse the plankton population [26]. This model is a 0D model and forms the basis of the further research in this report. To be able to use it, first the model of Steele and Henderson is explained and analysed.

2.1. Predator-Prey model

A model to describe a plankton population generally has the form of a predator-prey model:

$$\frac{dP}{dt} = \text{uptake - grazing} \tag{2.1}$$

$$\frac{dZ}{dt} = \text{growth - mortality} \tag{2.2}$$

P and Z represent the concentration of nitrogen (N) representing respectively phytoplankton and zooplankton in mg/m^3. Here phytoplankton represents the prey in the model. The mass of phytoplankton increases by the uptake of nutrients and decreases due to the grazing by its predator, zooplankton. Part of the grazing is converted into the growth of zooplankton. The mass of zooplankton decreases due to its mortality.

Steele and Henderson use the following equations in their article:

$$\frac{dP}{dt} = I(t)f(P) - Zg(P) \tag{2.3}$$

$$\frac{dZ}{dt} = \alpha g(P)Z - \alpha h(Z)Z \tag{2.4}$$

Here, $I(t)$ represents the light intensity over time. The factor α tells how much of the grazing is actually converted into growth, and is a conversion factor from phytoplankton to zooplankton. The functions $f(P)$, $g(P)$ and $h(Z)$ are given by:

$$f(P) = \beta P(1 - \frac{P}{\gamma}) \tag{2.5}$$

$$g(P) = \frac{\lambda P^n}{\mu + P^n}, \quad n = 1,2 \tag{2.6}$$

$$h(Z) = \delta Z^{m-1}, \quad m = 1,2 \tag{2.7}$$

These equations are based on commonly used functions that are empirical parametrizations of biological phenomena [2]. A lot of parameters are introduced in these functions, these should be clarified. The parameters β, λ and δ in the report of Steele and Henderson correspond to a time scale of 3 days. For further use of this model in combination with convection and diffusion, these parameters are rescaled to a time scale of 1 second. This is done by dividing the terms by 3600s/h $\cdot$ 24h/day $\cdot$ 3days.

- β (1/s) describes the slope of the function $f(P)$ when P is small. Furthermore, together with γ it determines the maximum value of $f(P)$ which equals $\frac{\beta\gamma}{4}$. The function $f(P)$ has impact on the growth term. This means the higher β, the greater the effect of $f(P)$, and thus the greater the growth of phytoplankton.
- γ (mg/m^3) is the density value for which the phytoplankton is saturated, or the maximum value of phytoplankton. This means that at that value, no more phytoplankton can grow. This is caused by the fact that the sun can no longer penetrate the water, due to the high concentration of phytoplankton.
- λ (1/s) describes the maximum value of the function $g(P)$, thus it indicates the influence of grazing on the system.
- μ ((mg/m^3)^n) is the half-saturation value of the grazing. If P^n equals μ, the grazing function equals $\frac{\lambda}{2}$. This means that the zooplankton eats $\frac{\lambda}{2}$ times its weight in 1 second.
- δ ((m^3/mg)$^{m-1}$/s) is the predation parameter and indicates how much effect predation has on the system.

There are nine parameters in these equations: P, Z, t, α, β, γ, δ, λ and μ. In addition $m = 1,2$ and $n = 1,2$. The system can be expressed with less parameters, by rewriting the system to a dimensionless form. This derivation is given in appendix A. However, the number of parameters can only be reduced by 2. Therefore, the Steele and Henderson model is used with the following simplification. To simplify the analysis, Steele and Henderson set β and λ to 1/3 days and μ to 1 (mg/m^3)^n . In addition γ is substituted by c, the saturation value, and δ is substituted by a, the mortality factor. This renders the following set of equations:

$$f(P) = P(1 - \frac{P}{c}) \tag{2.8}$$

$$g(P) = \frac{P^n}{1+P^n}, \quad n = 1,2 \tag{2.9}$$

$$h(Z) = aZ^{m-1}, \quad m = 1,2 \tag{2.10}$$

Knowing the functions and understanding its parameters, the separate terms are further analysed below.

2.1.1. Uptake

The uptake of phytoplankton is given by the term $I(t)f(P)$. In this report, it is considered that there are always enough nutrients available in the water, which means the nutrients are no limiting factor on the growth. This can be assumed if the mixing of the water is well enough and if enough nutrients are present.

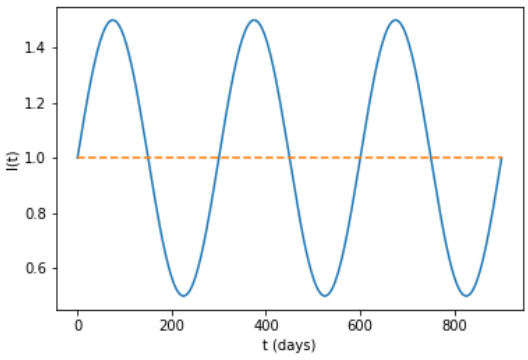

Figure 2.1: Light intensity function. In blue the light intensity fluctuating due to the seasons. In orange the light intensity set to 1.

Here $I(t)$ is the light intensity. The uptake of phytoplankton is influenced by the light intensity, as light is needed for photosynthesis. The higher the intensity the more photosynthesis, thus the more uptake of phytoplankton. To check if the model creates the same results as the model of Steele and Henderson, the light intensity is modelled the same way by $I(t) = 1 + 0.5sin(\frac{2\pi}{300 \cdot 24 \cdot 3600}t)$. This means that the intensity has a period

of 300 days, almost a year. The mean of the intensity is 1 and its amplitude is 0.5. In winter, the intensity is lowest (0.5), in summer the highest (1.5), which is depicted by the sinus in figure 2.1. The light intensity renders a factor by which $f(P)$ is multiplied. To simplify the model, the light intensity can alternatively be set to a constant value of 1. Then, the light intensity does not affect the system. This makes the analysis of the other terms in the system easier.

$f(P)$ is the self shadowing function and is given by equation 2.8. The function displays the potential growth of phytoplankton. After the normalisation the function still has the parameter c. Steele and Henderson set $c = 10\text{mg/m}^3$. The corresponding function is plotted in figure 2.2.

It can be seen that $f(P)$ varies from 0 to $1{\cdot}10^{-5}\text{mg/m}^3/s$. These values are realistic as the typical growth of phytoplankton in one day is between 0 and 1 mg/m^3 [24]. At the start, the function is more or less linear: the uptake experiences exponential growth: the more phytoplankton there is, the more phytoplankton is added. This can be compared to growth with exponential behaviour in nature. Exponential growth would lead to an immense amount of phytoplankton. However, there is a limit: the saturation value c. This limit occurs due to the penetration of sunlight. At a certain density of phytoplankton, sunlight can no longer penetrate the water and therefore can no longer stimulate growth by photosynthesis. Due to this limit, the function has the shape of a parabola, which has value zero at 0 mg/m^3 and $c = 10\text{mg/m}^3$ and its peak at $c/2$ with maximum growth rate $c/4$ per 3 days.

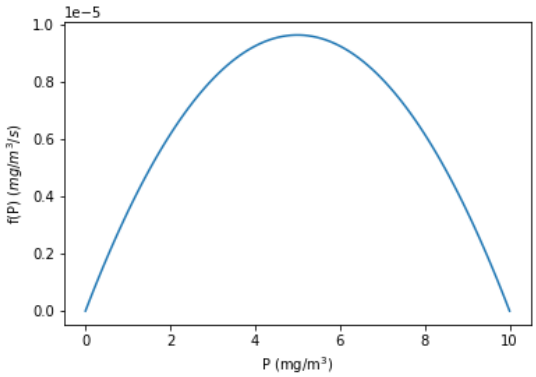

Figure 2.2: Self shadowing function.

2.1.2. Grazing

The grazing is described by the term $Zg(P)$. Here $g(P)$ is the grazing function. The grazing function shows how much phytoplankton is eaten by zooplankton; how many times the zooplankton eats its own weight in 3 days. The grazing function is multiplied by Z, the number of zooplankton.

The grazing function $g(P)$ is given by equation 2.9 and is depicted in figure 2.3. As it displays a proportion, the function takes a value between 0 and 1. If there is no phytoplankton, no phytoplankton can be grazed: the function starts at (0,0). Next, as the half saturation value μ was chosen to be equal to 1 $(\text{mg/m}^3)^n$, the function crosses $(1, \frac{1}{2})$. Lastly, the more phytoplankton there is, the more the function approaches 1, creating an asymptote. Overall, the grazing function depicts that the more phytoplankton there is, the more phytoplankton is grazed per amount of zooplankton, limiting up to a maximum: its own weight in 3 days ($\frac{1}{3600 \cdot 24 \cdot 3}$ times its own weight per second).

Steele and Henderson give two options for the grazing function, $n = 1$ or $n = 2$. Both functions have the characteristics listed above. For $n = 1$, the function has a hyperbolic form, while for $n = 2$ it has an S-form. For $n = 1$, the growth up to the half saturation value is faster. But onwards, the graph matching $n = 2$ converges faster to the limit 1. Another difference is that for $n = 2$ the derivative at $P = 0$ is zero. Which means that if there is little phytoplankton, almost no grazing occurs.

2.1.3. Growth

The growth of zooplankton is dependent on the grazing and is given by $\alpha g(P)Z$. How $g(P)Z$ behaves was discussed in subsection 2.1.2. The factor α is a constant between 0 and 1. It denotes how much of the grazing is converted into zooplankton mass. The other part of the grazing is for example converted into energy. The factor has no unit as it converts P to Z which are expressed in the same unit.

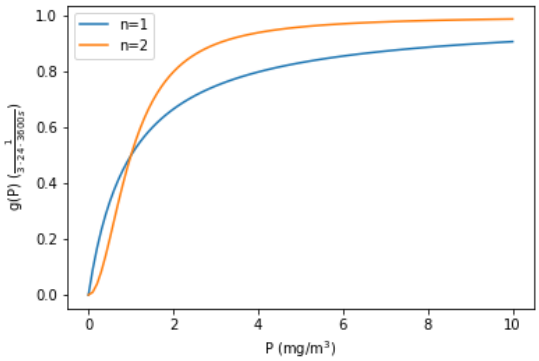

Figure 2.3: Grazing function for $n = 1$ and $n = 2$.

2.1.4. Mortality

The mortality term is given by $\alpha h(Z)Z$. Here the function $h(Z)$, see equation 2.10, is the mortality rate. The mortality rate describes which part of the zooplankton dies, therefore it has to be multiplied by the number of zooplankton to get the total mortality. Here all death options are considered: natural death, but also death by being eaten. α represents the conversion from phytoplankton to zooplankton.

The function for the mortality rate is shown in figure 2.4. Steele and Henderson give two options for the mortality rate: $m = 1$ and $m = 2$. $m = 1$ yields a constant mortality rate a. This means that always the same proportion of zooplankton will die. However, for $m = 2$, the mortality rate linearly depends on the number of zooplankton: aZ. The more zooplankton there is, the higher the mortality rate. The choice for this mortality rate can be justified by the thought that the more zooplankton there is, the more natural enemies it will attract.

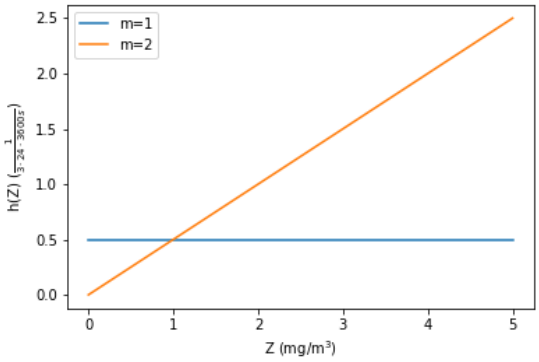

Figure 2.4: Mortality function for $m = 1$ and $m = 2$.

2.2. Comparing models

To illustrate this model some solutions are plotted. The parameters and initial conditions are chosen in such a way that some plots can be compared to the results of Steele and Henderson to validate the implementation of the model. By integrating the time derivatives solutions for the plankton population can be computed. For all possible combinations of $m = 1,2$ and $n = 1,2$ and $I(t)$ varying in time the solution is plotted in figure 2.5. Here $a = 0.7$ and the initial position is (P,Z) = (1,1).

The figure 2.5b is also plotted in the article of Steele and Henderson. The plots are identical, therefore it can be concluded that the programmed model is correct. The axes are labeled, as this was not added in Steele and Henderson. Furthermore, the equilibrium solutions Z^* and P^* are added in subplots 2.5a and 2.5b. What Z^* and P^* mean and how they are derived is described in section 2.3.

In all subplots in figure 2.5, the solutions for Z and P are periodic, with a period of 300 days. This periodicity is caused by the light intensity, which has the same periodicity.

The effect of m and n can be analysed using figure 2.5.

Comparing subplot 2.5a and 2.5b, the effect of n can be studied. Both subplots have an additional periodicity. The frequency of this periodicity is higher for $n = 2$, furthermore the peaks are sharper. In both cases the phytoplankton and zooplankton follow each other: if there is a lot of phytoplankton the zooplankton population increases. Due to more zooplankton, the phytoplankton decreases. This decrease also causes less possible food for the zooplankton, due to which its population decreases. Then, there is more room for the phytoplankton to grow, thus ending up with a lot of phytoplankton again. This cycle repeats itself. Such a cycle is expected in a predator-prey model. The difference in frequency and sharpness is caused by the effect of n on the grazing term. As has been seen in figure 2.3, the grazing function with $n = 2$ converges faster to 1, therefore the grazing term will be higher for $n = 2$ if $P > 1$. This causes the steeper descending parts in P and steeper ascending parts in Z in subplot 2.5b.

Comparing subplot 2.5a and 2.5c, the effect of m can be studied. In subplot 2.5c no additional periodicity can be seen, the solution converges to its equilibrium solution. With $m = 2$ the mortality term is higher than with $m = 1$ as soon as $Z > 1$. The number of zooplankton is therefore expected to have lower peaks, which can be seen indeed.

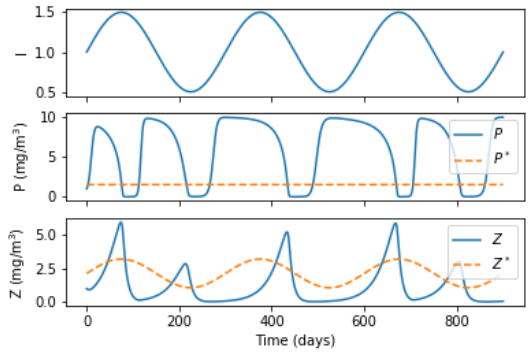

(a) Model run for $m = 1$ and $n = 1$.

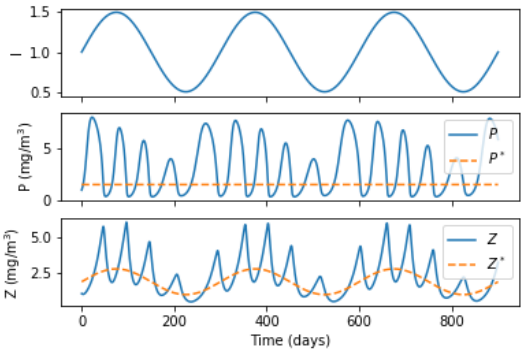

(b) Model run for $m = 1$ and $n = 2$.

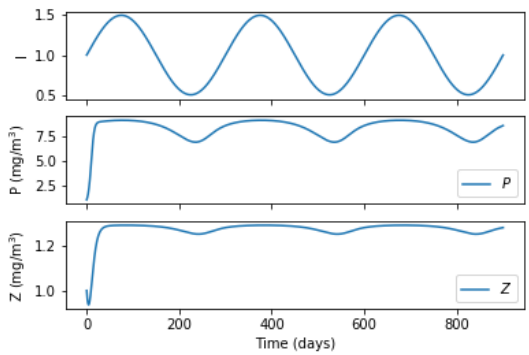

(c) Model run for $m = 2$ and $n = 1$.

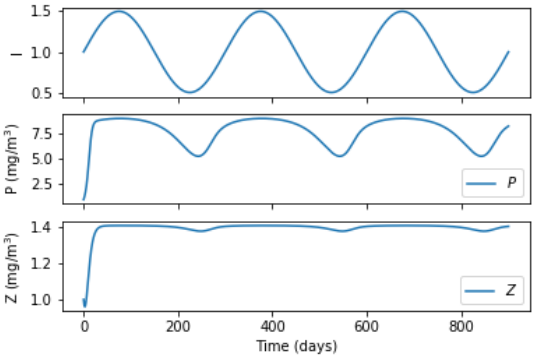

(d) Model run for $m = 2$ and $n = 2$.

Figure 2.5

2.3. Equilibrium

In the results of the Steele and Henderson model, it can be seen that the solution keeps repeating the same pattern. It is interesting to study these patterns in more detail. From now on for simplicity the light intensity is set to a constant: $I(t) = 1$

First of all the equilibrium points have to be determined. This can be achieved by equating the time derivatives to zero: $\frac{dP}{dt} = 0$, $\frac{dZ}{dt} = 0$. If both time derivatives are zero in the same point, this point is called an equilibrium point. The equilibrium points can be plotted by plotting the functions derived from $\frac{dP}{dt} = 0$ and $\frac{dZ}{dt} = 0$ in the form $Z(P)$. If Z is independent of P, the value of P is denoted. The resulting functions when $I(t) = 1$ are displayed in table 2.1. In general, the equilibria solutions P^* and Z^* are given by the following equations:

$$I(t)f(P^*) - Z^* g(P^*) = 0 \tag{2.11}$$

$$\alpha g(P^*)Z^* - \alpha h(Z^*)Z^* \tag{2.12}$$

resulting in

$$Z^* = \frac{I(t)f(P^*)}{g(P^*)} \tag{2.13}$$

$$g(P^*) = h(Z^*) \tag{2.14}$$

	$m=1,\ n=1$	$m=1,\ n=2$	$m=2,\ n=1$	$m=2,\ n=2$
$\frac{dP}{dt}=0$	$Z=(1-\frac{P}{c})(1+P)$	$Z=\frac{1}{P}(1-\frac{P}{c})(1+P^2)$	$Z=(1-\frac{P}{c})(1+P)$	$Z=\frac{1}{P}(1-\frac{P}{c})(1+P^2)$
$\frac{dZ}{dt}=0$	$P=\frac{a}{1-a}$	$P=\sqrt{\frac{a}{1-a}}$	$Z=\frac{P}{(1+P)a}$	$Z=\frac{P^2}{(1+P^2)a}$

Table 2.1: Functions derived from $\frac{dP}{dt}=0$ and $\frac{dZ}{dt}=0$ in the form $Z(P)$ and $P(a)$ for combinations of $m=1,2$ and $n=1,2$.

Having determined the stability points, the next step is to determine what kind of stability point it is: a stable, unstable or saddle point. This can be done using the linear stability analysis [19]. As a start, the Jacobian J for the equilibrium point has to be determined:

$$J = \left[\begin{array}{cc} \frac{\partial}{\partial P}(\frac{dP}{dt}) & \frac{\partial}{\partial Z}(\frac{dP}{dt}) \\ \frac{\partial}{\partial P}(\frac{dZ}{dt}) & \frac{\partial}{\partial Z}(\frac{dZ}{dt}) \end{array}\right]\Bigg|_{Z=Z^*,P=P^*} \tag{2.15}$$

If the eigenvalues corresponding to the Jacobian both have negative real part, it is a stable point. This means the solution converges to this point. If at least one of the eigenvalues has negative real part, it is an unstable point. If one eigenvalue has negative real part and the other positive real part, it is a saddle point.

For all possible combinations of m and n, the equilibrium points are displayed in figure 2.6. Figure 2.6 shows the lines $\frac{dP}{dt}=0$ (solid line) and $\frac{dZ}{dt}=0$ (dashed lines). Here the three dashed lines correspond to different values of a, to depict the differences caused by this parameter. The points where these lines intersect are the equilibrium points. The saddle points are depicted as a triangle, unstable points as crosses and stable points as circles. The layout of figure 2.6 is chosen so that it is similar to the figure of Steele and Henderson. However, in figure 2.6 the axes are labeled, the saddle points are differentiated from the other unstable points and the values used for a are notated.

In subplot 2.6c and 2.6d it can be seen that there are situations where 3 equilibrium points are found. What happens in such a situation is discussed in subsection 2.3.2.

2.3.1. Phase portrait

One way to visualise the solutions and its equilibria is by plotting a phase portrait. Here, for every point the value of the two derivatives is computed. These are displayed as an arrow, with the length and direction representing the value of the two derivatives added. Following these arrows the path of a solution can be visualised. For $a=0.5$, the solutions starting from different initial conditions are displayed in figure 2.7. For the subplots different initial conditions are plotted in different colors to indicate what happens. The starting point of a line is the used initial condition.

The dashed lines represent the solutions for $\frac{dP}{dt}=0$ and $\frac{dZ}{dt}=0$, the intersection point is the equilibrium. It can be seen that when the equilibrium point is a stable point (subplots 2.7b, 2.7c and 2.7d), the solutions converge to the equilibrium point. It is noticeable that the solutions first converge to one of the dashed lines and then converge to the equilibrium point. This suggests that one of the two differential equations converges faster than the other.

In subplot 2.7a the equilibrium point is an unstable point. The solutions all move towards the y-axis, from there on all solutions follow the same cycle: the limit cycle. The limit cycle is computed by letting a solution run for a long time. By that time the solution will have approached the limit cycle.

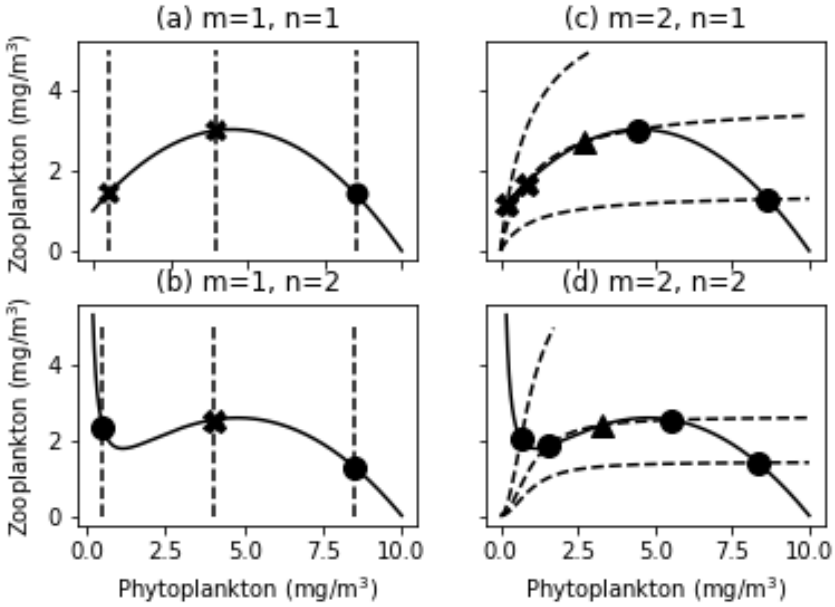

Figure 2.6: Equilibrium lines $\frac{dP}{dt} = 0$ (solid line) and $\frac{dZ}{dt} = 0$ (dashed lines) with equilibrium points. The saddle points are depicted as a triangle, unstable points as crosses and stable points as circles. The lay out is chosen to reproduce the figure of Steele and Henderson. The dashed lines in (a) and (b) correspond to P =0.5, 4 and 8.5. In (c) the dashed lines correspond to a = 0.15, 0.27 and 0.7. In (d) the dashed lines correspond to a = 0.15, 0.38 and 0.7

2.3.2. Bifurcation diagram

In figure 2.6 it was seen that the equilibrium depends on a. To show which value of a gives rise to which equilibrium, bifurcation diagrams are used. Here for each value of a the value of P^* is plotted. Furthermore, to illustrate the solution the minimum and maximum value of P are plotted for a period of time after the solution has converged to its equilibrium. If the three lines follow the same path, the equilibrium point is stable. When the three lines split the equilibrium point is unstable and a limit cycle occurs. Then, the minimum and maximum value of P give insight in the range of the limit cycle. It is chosen to plot P, because phytoplankton has a direct effect on the oxygen level on earth. Furthermore, similar trends in the bifurcation diagrams occur for Z.

The three lines are all computed numerically. For the P_{min} and P_{max}, this is the only option. However this leads to a certain inaccuracy. For example in subplot 2.8b this inaccuracy can be noticed: around $a = 1$, the three lines slightly deviate from one another. However, the equilibrium is stable here. The deviation is caused by the fact that the function for determining the limit cycle has not converged close enough to the equilibrium point yet. This problem could be helped by letting the solution run for a longer time, and therefore find a more precise solution.

In subplots 2.8a and 2.8b, the stable and unstable part can be clearly differentiated and smoothly merge into each other. In subplots, the transition is different, this is caused by the possibility of three equilibrium points for one a as seen in subplot 2.6c and 2.6d. For such a case P^* is sorted to be a smooth function: first all the lower equilibrium points of the solution are added, then the middle and afterwards the highest. The equilibrium solution makes an S-shape. However the P_{min} and P_{max} immediately converge to the highest equilibrium, which means the solution converges to that point. It could however be that there are multiple solutions, that depends on the initial condition. To investigate this, for both subplot 2.8c and 2.8d a phase portrait is made. These can be found in figure 2.9.

In subplot 2.9a there are three different equilibrium points: an unstable point, a saddle point and a stable point. The solutions all converge to the stable point. A limit cycle could be expected around the unstable point, as this happens when there is only an unstable point. However this is not detected. A cycle seems to form, but ultimately the solution converges to the stable point as well.

In subplot 2.9b there is another pattern of equilibrium points: two stable points with in between a saddle point. Here, to which stable point the solution converges depends on the initial condition. In figure 2.8d, the chosen initial condition converged to the upper stable point.

As a correction of figures 2.8c and 2.8d figures 2.10a and 2.10b can be made. In figure 2.10a there is little

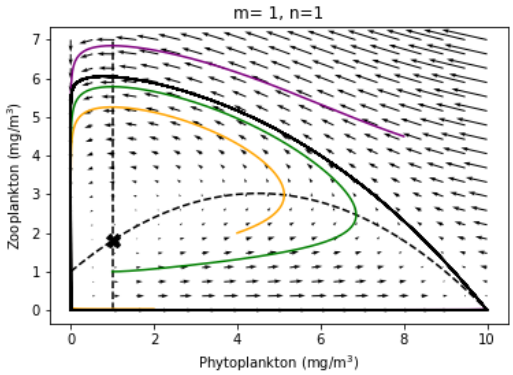

(a) Phase portrait for $m = 1$ and $n = 1$ with solutions corresponding to the initial conditions (P,Z) = (4,2) (yellow), (P,Z) = (1,1) (green) and (P,Z) = (8,4.5) (purple). The limit cycle is given by the thick black line.

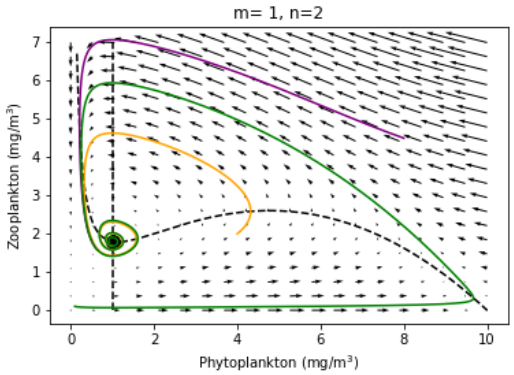

(b) Phase portrait for $m = 1$ and $n = 2$ with solutions corresponding to the initial conditions (P,Z) = (4,2) (yellow), (P,Z) = (0.1,0.1) (green) and (P,Z) = (8,4.5) (purple).

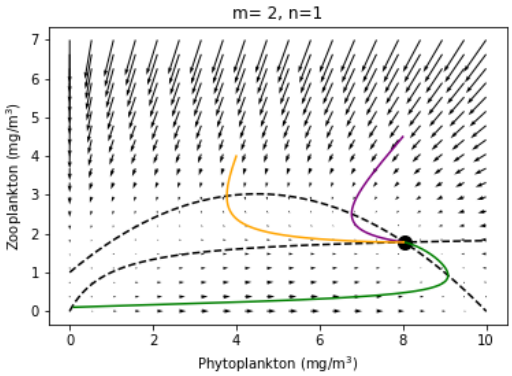

(c) Phase portrait for $m = 2$ and $n = 1$ with solutions corresponding to the initial conditions (P,Z) = (4,4) (yellow), (P,Z) = (0.1,0.1) (green) and (P,Z) = (8,4.5) (purple).

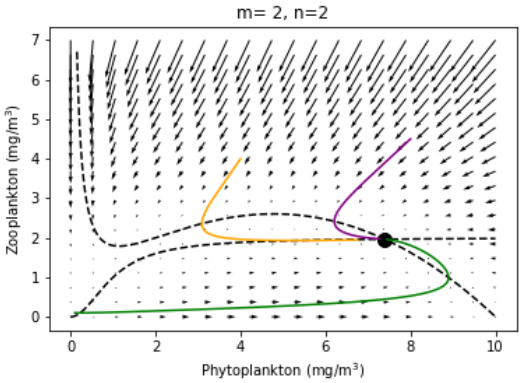

(d) Phase portrait for $m = 2$ and $n = 2$ with solutions corresponding to the initial conditions (P,Z) = (4,4) (yellow), (P,Z) = (0.1,0.1) (green) and (P,Z) = (8,4.5) (purple).

Figure 2.7

change as two of the three equilibrium points are unstable. The unstable P^* are displayed by the dashed line. In figure 2.10b the difference between stable and unstable equilibrium points is displayed. The figure can be interpreted in the following way: starting for a low value of a, the left stable line will be followed, in the section with three points as well. However once having an a greater than the one equaling three points, the solution will skip to the other stable line on the right. Now, once on this stable line, decreasing a, the right stable line will be followed, in the section with three points as well. Thus once surpassing a point, it will be harder to get back to a previous situation.

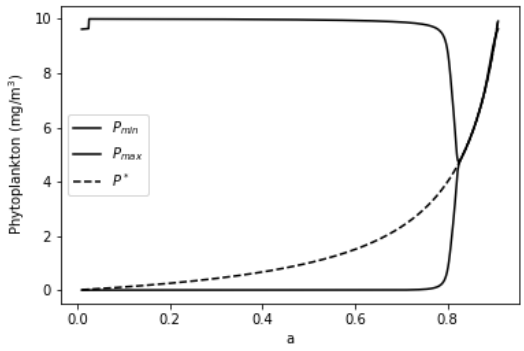

(a) Bifurcation diagram for $m = 1$ and $n = 1$.

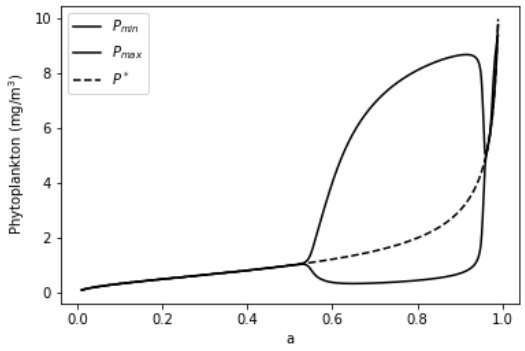

(b) Bifurcation diagram for $m = 1$ and $n = 2$.

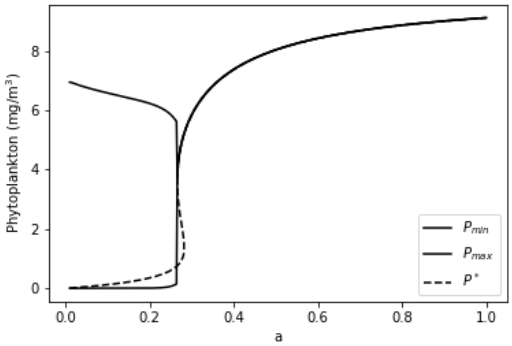

(c) Bifurcation diagram for $m = 2$ and $n = 1$.

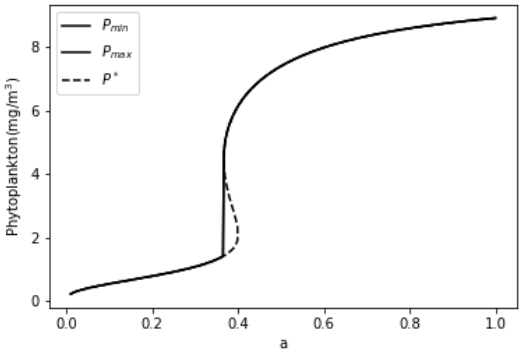

(d) Bifurcation diagram for $m = 2$ and $n = 2$.

Figure 2.8

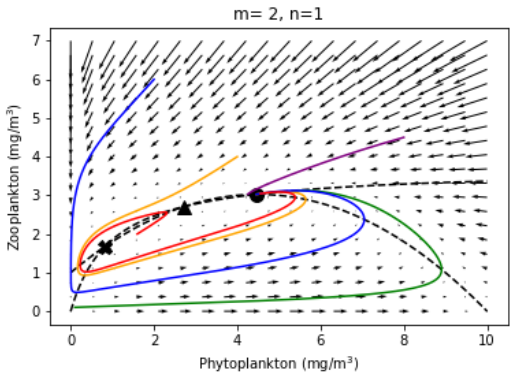

(a) Phase portrait for $m = 2$ and $n = 1$, with $a = 0.27$

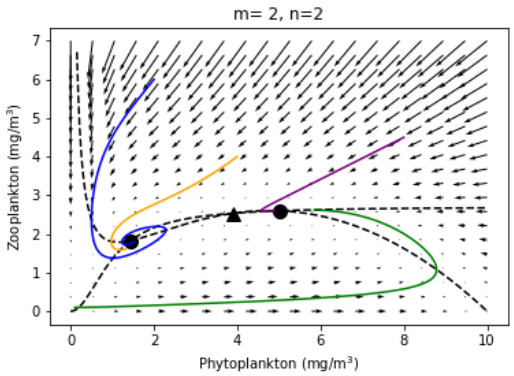

(b) Phase portrait for $m = 2$ and $n = 2$, with $a = 0.37$

Figure 2.9

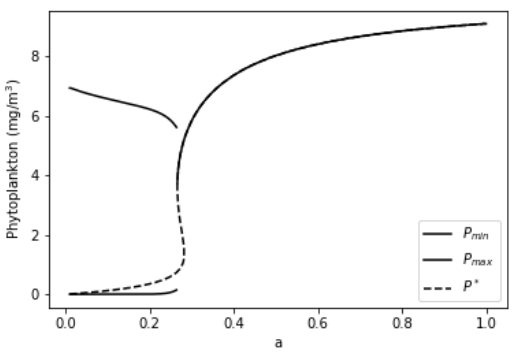

(a) Corrected bifurcation diagram for $m = 2$ and $n = 1$.

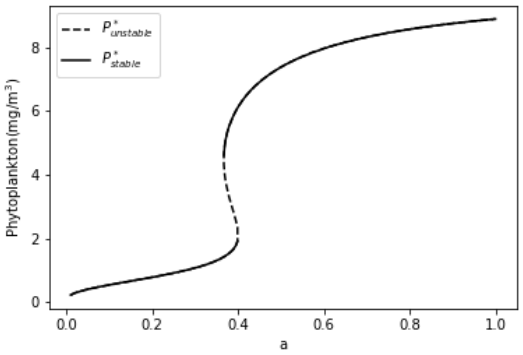

(b) Corrected bifurcation diagram for $m = 2$ and $n = 2$.

Figure 2.10

3

Convection and diffusion

In this chapter the 0D model of Steele and Henderson is expanded to a 2D model. The model configuration is inspired by the west coast of Portugal. First of all, the assumptions made about such a coastal area are given and explained. Next, the convection and diffusion are incorporated in the model. Then, the parameters used in the model are discussed: some are determined by literature research, others are variable. The impact of the variables is expressed by dimensionless numbers and timescales. Lastly, the model is analysed. First, the cases where only one of the processes (convection, diffusion or predator-prey) acts are validated, next more complicated situations are analysed and discussed.

3.1. Coastal area of an ocean

The expanded model is based on a coastal area of an ocean. Such an area is depicted in figure 3.1a. The area is considered to be a rectangle. The boundary $y = 0$ represents the coast. A current parallel to the coast is considered. This current flows in the x-direction. Furthermore, it is considered that the plankton mixes due to the turbulence, waves and other flows in the water. This dispersion is modeled with diffusion in the x and y-direction.

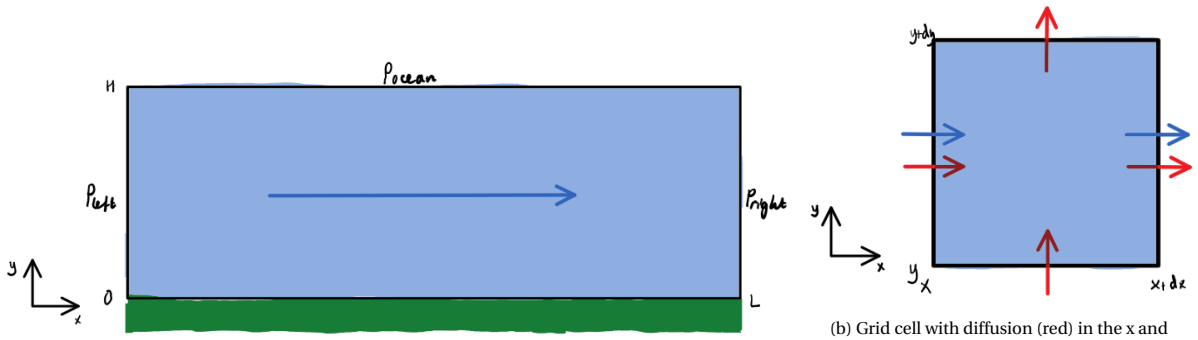

(a) Schematic of coastal area of an ocean with current parallel to the coast.

(b) Grid cell with diffusion (red) in the x and y-direction and convection (blue) in the x-direction.

Figure 3.1

In specific, a cliff coast is considered. Then, it can be considered that directly off the coast the depth of the water plunges. There is no zone in which the waves sway back and forth, in other words there is a boundary which the water cannot pass. Furthermore, a coastal area is shallow so sunlight reaches the bottom. Therefore, a depth integrated model is considered. In addition, in coastal areas there are typically sufficient nutrients [7], so there is no additional limiting factor to the growth of phytoplankton.

This coastal area model gives rise to the boundary conditions used in the system. In the open ocean the concentration of phytoplankton is relatively low, therefore the boundary at $y = H$ is set to:

$$c(x, H, t) = c_{ocean} \tag{3.1}$$

where c_{ocean} is small and c represents either P or Z.

The boundaries at $x = 0$ and $x = L$ are considered to be constant:

$$c(0, y, t) = c_{left} \tag{3.2}$$

$$c(L, y, t) = c_{right} \tag{3.3}$$

Lastly, at the coast ($y = 0$) no water, and therefore no plankton can pass. This gives rise to the following boundary condition:

$$\frac{\partial c(x, 0, t)}{\partial y} = 0 \tag{3.4}$$

3.2. Model convection and diffusion

The mentioned current and diffusion have to be incorporated in the model. To do this, the mass balance over a piece of water of the form dx by dy is taken, the depth of the water is h. In general the equation for the mass balance is:

$$\frac{d}{dt}(Vc) = \text{flow in - flow out + production} \tag{3.5}$$

Where $V = h \cdot dx \cdot dy$ is the volume of the piece of water. In figure 3.1b the flows are depicted: in the x-direction there is flow in and flow out due to convection and diffusion, in the y-direction solely due to diffusion. The production term is described by the model of Steele and Henderson given in equations 2.3 and 2.4 multiplied by the volume V.

For the convection, the velocity v at the boundary is multiplied by the concentration c and the surface of the boundary ($h \cdot dy$) to determine the flow in and flow out. Thus, the mass flow due to convection is expressed by the term $h \cdot v \cdot c \cdot dy$.

The diffusion is caused by differences in concentration. Due to these differences, a flow from higher to lower concentrations arises. The flow can be computed using Fick's law [27]:

$$\phi'' = -D\frac{\partial c}{\partial x} \tag{3.6}$$

Multiplying this by the surface of the boundary ($h \cdot dy$), gives the mass flux in the x-direction caused by diffusion. The diffusion is determined by the diffusion coefficient D and the concentration gradient in the x-direction. The same applies in the y-direction, here the x and y are interchanged.

All terms together form the following mass balance over a small volume. Here the depth, velocity and diffusion term are considered to be dependent on x and y.

$$\begin{aligned}
\frac{\partial}{\partial t}\Big(\int_x^{x+dx}\int_y^{y+dy} h(x,y)c(x,y)dxdy\Big) &= \int_y^{y+dy} h(x,y)v(x,y)c(x,y)dy - \int_y^{y+dy} h(x,y)D(x,y)\left.\frac{\partial c(x,y)}{\partial x}\right|_x dy \\
&- \int_x^{x+dx} h(x,y)D(x,y)\left.\frac{\partial c(x,y)}{\partial y}\right|_y dx - \int_y^{y+dy} h(x+dx,y)v(x+dx,y)c(x+dx,y)dy \\
&- \int_y^{y+dy} h(x+dx,y)D(x+dx,y)\left.\frac{\partial c(x,y)}{\partial x}\right|_{x+dx} dy - \int_x^{x+dx} h(x,y+dy)D(x,y+dy)\left.\frac{\partial c(x,y)}{\partial y}\right|_{y+dy} dx \\
&+ (\text{predator-prey terms})h(x,y)dxdy
\end{aligned}$$

Here c represents either phytoplankton (P) or zooplankton (Z) and the predator-prey terms are given by equations 2.3 and 2.4 respectively.

The integrals in this equation make it hard to compute. To get rid of the integrals the mean value theorem is used in combination with Lipschitz continuity [16]. The mean value theorem is stated in equation 3.7, where $\tilde{x}$ is a value between x and $x + dx$.

$$\int_x^{x+dx} f(x)dx = f(\tilde{x})dx \tag{3.7}$$

Now using that the function is lipschitz continuous, for any $\epsilon > 0$ there is a dx sufficiently small such that:

$$|f(x) - f(\tilde{x})| < \epsilon \quad \text{for all x in } (x, x + dx) \tag{3.8}$$

Therefore any value of $(x, x+dx)$ can be chosen for $\tilde{x}$. For simplicity, x is chosen.
To derive the system of equations the following steps are executed:

- All integrals can be approximated by multiplying the integrated function by the area of integration using the mean value theorem in combination with lipschitz continuity.
- The volume $h(x,y)dxdy$ can be taken in front of the time derivative, as it is independent of time. Furthermore, the equation is divided by $h(x,y)dxdy$ and reshuffled.
- The limits $dx \to 0$ and $dy \to 0$ are taken. Then, the equation can be rewritten with partial derivatives.
- $h(x,y)v(x,y)$ can be taken in front of the x derivative. The water flow is independent of x: $h(x,y)v(x,y) =$ constant. There are no places where the water can pile up or disappear.

The complete derivation that is described with steps in between can be found in appendix B. The following system of equations is found:

$$\frac{\partial P(x,y)}{\partial t} = -v(x,y)\frac{\partial P(x,y)}{\partial x} + \frac{1}{h(x,y)}\frac{\partial}{\partial x}(h(x,y)D(x,y)\frac{\partial P(x,y)}{\partial x}) + \frac{1}{h(x,y)}\frac{\partial}{\partial y}(h(x,y)D(x,y)\frac{\partial P(x,y)}{\partial y}) + I(t)f(P) - Zg(P) \tag{3.9}$$

$$\frac{\partial Z(x,y)}{\partial t} = -v(x,y)\frac{\partial Z(x,y)}{\partial x} + \frac{1}{h(x,y)}\frac{\partial}{\partial x}(h(x,y)D(x,y)\frac{\partial Z(x,y)}{\partial x}) + \frac{1}{h(x,y)}\frac{\partial}{\partial y}(h(x,y)D(x,y)\frac{\partial Z(x,y)}{\partial y}) + \alpha g(P)Z - \alpha h(Z)Z \tag{3.10}$$

To solve the system of equation, boundary conditions and initial conditions are needed. The boundary conditions are already given in equation 3.1, 3.2, 3.3 and 3.4. Here c represents either P or Z.
The initial conditions are:

$$c(x,y,0) = c_i \tag{3.11}$$

where again c represents either P or Z.

3.2.1. Spatial discretization

The system of equations given by equation 3.9 and 3.10 cannot be solved analytically. Therefore, it is necessary to approximate the solution numerically. To do this, the studied coastal area is represented by a grid with $N_x + 1$ points in the x-direction and $N_y + 1$ points in the y-direction. The gridpoints are equidistantly distributed, which means $\Delta x = L/N_x$ and $\Delta y = H/N_y$. For the numerical approximation backward differentiation is used for convection, central differentiation is used for diffusion [2]. Backward differentiation is used for convection to make sure the system is stable, also for large gridcell Péclet numbers (Pe = $\frac{v\Delta x}{D}$), however central differentiation is a more precise differentiation method. These differentiation methods equal to the following equations, where c represents either P or Z.

$$v\left.\frac{\partial c}{\partial x}\right|_{x_n} = v_{n,m}\frac{c_{n,m} - c_{n-1,m}}{\Delta x} + \mathcal{O}(\Delta x) \tag{3.12}$$

$$\frac{1}{h}\frac{\partial}{\partial x}(hD\frac{\partial c}{\partial x})\Big|_{x_n} = \frac{1}{h_{n,m}}\frac{h_{n+\frac{1}{2},m}D_{n+\frac{1}{2},m}c_{n+1,m} - (h_{n+\frac{1}{2},m}D_{n+\frac{1}{2},m} + h_{n-\frac{1}{2},m}D_{n-\frac{1}{2},m})c_{n,m} + h_{n-\frac{1}{2},m}D_{n-\frac{1}{2},m}c_{n-1,m}}{\Delta x^2} + \mathcal{O}(\Delta x^2) \tag{3.13}$$

$$\frac{1}{h}\frac{\partial}{\partial y}(hD\frac{\partial c}{\partial y})\Big|_{y_m} = \frac{1}{h_{n,m}}\frac{h_{n,m+\frac{1}{2}}D_{n,m+\frac{1}{2}}c_{n,m+1} - (h_{n,m+\frac{1}{2}}D_{n,m+\frac{1}{2}} + h_{n,m-\frac{1}{2}}D_{n,m-\frac{1}{2}})c_{n,m} + h_{n,m-\frac{1}{2}}D_{n,m-\frac{1}{2}}c_{n,m-1}}{\Delta y^2} + \mathcal{O}(\Delta y^2) \tag{3.14}$$

Here the value of the height and diffusion coefficient are needed in between the grid points. These are however unknown. To approximate these values the mean of the two closest grid points is taken:

$$h_{n\pm\frac{1}{2}} = \frac{h_{n\pm1} + h_n}{2} \tag{3.15}$$

Substituting the numerical approximations in the differential equations renders:

$$\begin{aligned}\frac{\partial P}{\partial t} &= \left(\frac{h_{n+\frac{1}{2},m}D_{n+\frac{1}{2},m}}{h_{n,m}\Delta x^2}\right)P_{n+1,m} + \left(\frac{h_{n,m+\frac{1}{2}}D_{n,m+\frac{1}{2}}}{h_{n,m}\Delta y^2}\right)P_{n,m+1} \\ &+ \left(-\frac{h_{n+\frac{1}{2},m}D_{n+\frac{1}{2},m} + h_{n-\frac{1}{2},m}D_{n-\frac{1}{2},m}}{h_{n,m}\Delta x^2} - \frac{h_{n,m+\frac{1}{2}}D_{n,m+\frac{1}{2}} + h_{n,m-\frac{1}{2}}D_{n,m-\frac{1}{2}}}{h_{n,m}\Delta y^2} - \frac{v_{n,m}}{\Delta x}\right)P_{n,m} \\ &+ \left(\frac{h_{n-\frac{1}{2},m}D_{n-\frac{1}{2},m}}{h_{n,m}\Delta x^2} + \frac{v_{n,m}}{\Delta x}\right)P_{n-1,m} + \left(\frac{h_{n,m-\frac{1}{2}}D_{n,m-\frac{1}{2}}}{h_{n,m}\Delta y^2}\right)P_{n,m-1} \\ &+ I(t)f(P_{n,m}) - Z_{n,m}g(P_{n,m})\end{aligned}$$

$$\begin{aligned}\frac{\partial Z}{\partial t} &= \left(\frac{h_{n+\frac{1}{2},m}D_{n+\frac{1}{2},m}}{h_{n,m}\Delta x^2}\right)Z_{n+1,m} + \left(\frac{h_{n,m+\frac{1}{2}}D_{n,m+\frac{1}{2}}}{h_{n,m}\Delta y^2}\right)Z_{n,m+1} \\ &+ \left(-\frac{h_{n+\frac{1}{2},m}D_{n+\frac{1}{2},m} + h_{n-\frac{1}{2},m}D_{n-\frac{1}{2},m}}{h_{n,m}\Delta x^2} - \frac{h_{n,m+\frac{1}{2}}D_{n,m+\frac{1}{2}} + h_{n,m-\frac{1}{2}}D_{n,m-\frac{1}{2}}}{h_{n,m}\Delta y^2} - \frac{v_{n,m}}{\Delta x}\right)Z_{n,m} \\ &+ \left(\frac{h_{n-\frac{1}{2},m}D_{n-\frac{1}{2},m}}{h_{n,m}\Delta x^2} + \frac{v_{n,m}}{\Delta x}\right)Z_{n-1,m} + \left(\frac{h_{n,m-\frac{1}{2}}D_{n,m-\frac{1}{2}}}{h_{n,m}\Delta y^2}\right)Z_{n,m-1} \\ &+ \alpha g(P_{n,m})Z_{n,m} - \alpha h(Z_{n,m})Z_{n,m}\end{aligned}$$

To compute the solutions of this system of equations, the vectors **P** and **Z** of lexicographic ordering are created, see equation 3.18. Due to the boundary conditions, $c_{0,m}$, $c_{N_x+1,m}$ and c_{n,N_y+1} are known and therefore not included in the lexicographic vectors.

With these lexicographic vectors, the following vector equations are formed:

$$\frac{\partial \mathbf{P}}{\partial t} = \mathbf{MP} + \mathbf{V} + I(t)f(\mathbf{P}) - \mathbf{Z}g(\mathbf{P}) \tag{3.16}$$

$$\frac{\partial \mathbf{Z}}{\partial t} = \mathbf{MZ} + \mathbf{W} + \alpha g(\mathbf{P})\mathbf{Z} - \alpha h(\mathbf{Z})\mathbf{Z} \tag{3.17}$$

Here **M** is a $N_x(N_y+1)$ by $N_x(N_y+1)$ matrix, representing the differentiation steps. This matrix is given in figure 3.2. **V** and **W** represent the impact of the three Dirac boundary conditions, see equation 3.18. The computation of the vectors and matrix is given in appendix C.

$$\mathbf{P} = \begin{bmatrix} P_{1,0} \\ P_{2,0} \\ \vdots \\ P_{N_x-1,0} \\ P_{N_x,0} \\ P_{1,1} \\ P_{2,1} \\ \vdots \\ P_{N_x-1,1} \\ P_{N_x,1} \\ \vdots \\ \vdots \\ P_{1,N_y} \\ P_{2,N_y} \\ \vdots \\ P_{N_x-1,N_y} \\ P_{N_x,N_y} \end{bmatrix} \quad \mathbf{Z} = \begin{bmatrix} Z_{1,0} \\ Z_{2,0} \\ \vdots \\ Z_{N_x-1,0} \\ Z_{N_x,0} \\ Z_{1,1} \\ Z_{2,1} \\ \vdots \\ Z_{N_x-1,1} \\ Z_{N_x,1} \\ \vdots \\ \vdots \\ Z_{1,N_y} \\ Z_{2,N_y} \\ \vdots \\ Z_{N_x-1,N_y} \\ Z_{N_x,N_y} \end{bmatrix} \quad \mathbf{V} = \begin{bmatrix} D_0^* P_{left} \\ 0 \\ \vdots \\ 0 \\ B_0^* P_{right} \\ D_1^* P_{left} \\ 0 \\ \vdots \\ 0 \\ B_1^* P_{right} \\ \vdots \\ \vdots \\ D_{N_y}^* P_{left} + C_1^* P_{ocean} \\ C_2^* P_{ocean} \\ \vdots \\ C_{N_x-1}^* P_{ocean} \\ B_{N_y}^* P_{right} + C_{N_x}^* P_{ocean} \end{bmatrix} \quad \mathbf{W} = \begin{bmatrix} D_0^* Z_{left} \\ 0 \\ \vdots \\ 0 \\ B_0^* Z_{right} \\ D_1^* Z_{left} \\ 0 \\ \vdots \\ 0 \\ B_1'^* Z_{right} \\ \vdots \\ \vdots \\ D_{N_y}^* Z_{left} + C_1^* Z_{ocean} \\ C_2^* Z_{ocean} \\ \vdots \\ C_{N_x-1}^* Z_{ocean} \\ B_{N_y}^* Z_{right} + C_{N_x}^* Z_{ocean} \end{bmatrix} \tag{3.18}$$

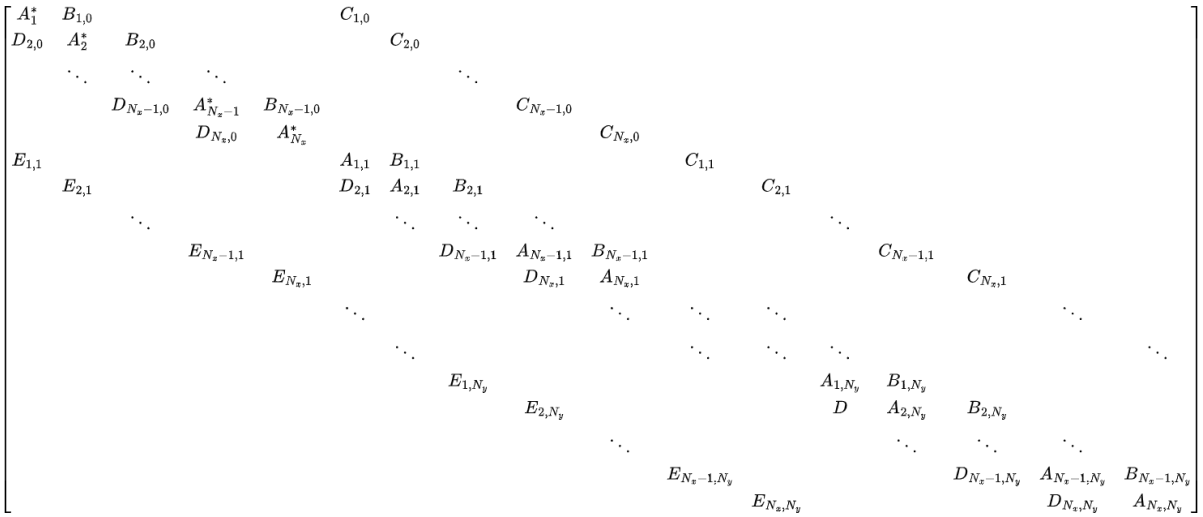

Figure 3.2: Matrix M

The used matrix and vector elements are given by:

$$A_{n,m} = -\frac{h_{n+\frac{1}{2},m}D_{n+\frac{1}{2},m} + h_{n-\frac{1}{2},m}D_{n-\frac{1}{2},m}}{h_{n,m}\Delta x^2} - \frac{h_{n,m+\frac{1}{2}}D_{n,m+\frac{1}{2}} + h_{n,m-\frac{1}{2}}D_{n,m-\frac{1}{2}}}{h_{n,m}\Delta y^2} - \frac{v_{n,m}}{\Delta x} \tag{3.19}$$

$$B_{n,m} = \frac{h_{n+\frac{1}{2},m}D_{n+\frac{1}{2},m}}{h_{n,m}\Delta x^2} \tag{3.20}$$

$$C_{n,m} = \frac{h_{n,m+\frac{1}{2}}D_{n,m+\frac{1}{2}}}{h_{n,m}\Delta y^2} \tag{3.21}$$

$$D_{n,m} = \frac{h_{n-\frac{1}{2},m}D_{n-\frac{1}{2},m}}{h_{n,m}\Delta x^2} + \frac{v_{n,m}}{\Delta x} \tag{3.22}$$

$$E_{n,m} = \frac{h_{n,m-\frac{1}{2}}D_{n,m-\frac{1}{2}}}{h_{n,m}\Delta y^2})Z_{n,m-1} \tag{3.23}$$

$$A^*_n = -\frac{h_{n+\frac{1}{2},0}D_{n+\frac{1}{2},0} + h_{n-\frac{1}{2},0}D_{n-\frac{1}{2},0}}{h_{n,0}\Delta x^2} - \frac{h_{n,\frac{1}{2}}D_{n,\frac{1}{2}}}{h_{n,0}\Delta y^2} - \frac{v_{n,0}}{\Delta x} \tag{3.24}$$

$$B^*_m = \frac{h_{N_x+\frac{1}{2},m}D_{N_x+\frac{1}{2},m}}{h_{N_x,m}\Delta x^2} \tag{3.25}$$

$$C^*_n = \frac{h_{n,N_y+\frac{1}{2}}D_{n,N_y+\frac{1}{2}}}{h_{n,N_y}\Delta y^2} \tag{3.26}$$

$$D^*_m = \frac{h_{\frac{1}{2},m}D_{\frac{1}{2},m}}{h_{1,m}\Delta x^2} + \frac{v_{1,m}}{\Delta x} \tag{3.27}$$

3.2.2. Time integration

After the spatial discretization, the next step is time integration. Multiple methods can be applied, two of them are forward and backward Euler. Forward Euler has the advantage that it yields 'simple' equations for $\mathbf{P}_{i+1}$ and $\mathbf{Z}_{i+1}$ expressed in $\mathbf{P}_i$ and $\mathbf{Z}_i$ as the method is explicit. Forward Euler and its resulting equation for $\mathbf{P}_{i+1}$ and $\mathbf{Z}_{i+1}$ are given by:

$$\frac{\mathbf{P}_{i+1} - \mathbf{P}_i}{\Delta t} = \mathbf{M}\mathbf{P}_i + \mathbf{V} + I(t_i)f(\mathbf{P}_i) - \mathbf{Z}_i g(\mathbf{P}_i) \tag{3.28}$$

$$\frac{\mathbf{Z}_{i+1} - \mathbf{Z}_i}{\Delta t} = \mathbf{M}\mathbf{Z}_i + \mathbf{W} + \alpha g(\mathbf{P}_i)\mathbf{Z}_i - \alpha h(\mathbf{Z}_i)\mathbf{Z}_i \tag{3.29}$$

$$\mathbf{P}_{i+1} = \mathbf{P}_i + \Delta t(\mathbf{M}\mathbf{P}_i + \mathbf{V} + I(t_i) f(\mathbf{P}_i) - \mathbf{Z}_i g(\mathbf{P}_i)) \tag{3.30}$$

$$\mathbf{Z}_{i+1} = \mathbf{Z}_i + \Delta t(\mathbf{M}\mathbf{Z}_i + \mathbf{W} + \alpha g(\mathbf{P}_i)\mathbf{Z}_i - \alpha h(\mathbf{Z}_i)\mathbf{Z}_i) \tag{3.31}$$

However, the disadvantage of forward Euler is the stability condition. To make sure the model is unconditionally stable, backward Euler could be used, as this is an implicit method. Backward Euler is given by:

$$\frac{\mathbf{P}_{i+1} - \mathbf{P}_i}{\Delta t} = \mathbf{M}\mathbf{P}_{i+1} + \mathbf{V} + I(t_{i+1}) f(\mathbf{P}_{i+1}) - \mathbf{Z}_{i+1} g(\mathbf{P}_{i+1}) \tag{3.32}$$

$$\frac{\mathbf{Z}_{i+1} - \mathbf{Z}_i}{\Delta t} = \mathbf{M}\mathbf{Z}_{i+1} + \mathbf{W} + \alpha g(\mathbf{P}_{i+1})\mathbf{Z}_{i+1} - \alpha h(\mathbf{Z}_{i+1})\mathbf{Z}_{i+1} \tag{3.33}$$

Due to the non-linearity of the predator-prey terms from Steele and Henderson, $\mathbf{P}_{i+1}$ and $\mathbf{Z}_{i+1}$ cannot be easily subtracted from these equations. To avoid this complication the predator-prey terms are taken explicitly. The diffusion and convection term are still taken implicitly, which leads to a partially implicit equation that can be used. Due to its partial implicity the integration is more stable. This results in the following equations:

$$\frac{\mathbf{P}_{i+1} - \mathbf{P}_i}{\Delta t} = \mathbf{M}\mathbf{P}_{i+1} + \mathbf{V} + I(t_i) f(\mathbf{P}_i) - \mathbf{Z}_i g(\mathbf{P}_i) \tag{3.34}$$

$$\frac{\mathbf{Z}_{i+1} - \mathbf{Z}_i}{\Delta t} = \mathbf{M}\mathbf{Z}_{i+1} + \mathbf{W} + \alpha g(\mathbf{P}_i)\mathbf{Z}_i - \alpha h(\mathbf{Z}_i)\mathbf{Z}_i \tag{3.35}$$

These equations can be rewritten to the following equations for $\mathbf{P}_{i+1}$ and $\mathbf{Z}_{i+1}$:

$$\mathbf{P}_{i+1} = (\mathbf{I} - \Delta t\mathbf{M})^{-1}(\mathbf{P}_i + \Delta t(\mathbf{V} + I(t_i) f(\mathbf{P}_i) - \mathbf{Z}_i g(\mathbf{P}_i))) \tag{3.36}$$

$$\mathbf{Z}_{i+1} = (\mathbf{I} - \Delta t\mathbf{M})^{-1}(\mathbf{Z}_i + \Delta t(\mathbf{W} + \alpha g(\mathbf{P}_i)\mathbf{Z}_i - \alpha h(\mathbf{Z}_i)\mathbf{Z}_i)) \tag{3.37}$$

This model is implemented. The used code can be found in appendix D.

3.3. Parameters

In this section the choices for the parameter values in the model are explained. Some values are chosen for simplicity, others are based on literature.

The number of grid points N_x and N_y determine the gridsize. Larger N_x and N_y equal a smaller gridsize and therefore a better numerical approximation. However, N_x and N_y also determine the size of the matrix in the numerical approximation. The larger this matrix is, the longer the running time of the model is. To have a reasonable running time $N_x = 200$ and $N_y = 80$ are used.

The number of time steps is chosen, such that the plankton population is modeled over more or less 3 years. The size of the time steps is chosen as large as possible to minimize the running time. However, the time step should be small enough so that the production terms are not unstable, therefore $dt = 20000$ s is used [2]. Furthermore, the larger the time step is. the larger the numerical error is.

The grid size and time step are both limited due to the running time of the model. To make the model more efficient parallel programming is used.

For simplicity the light intensity is set to a constant value of 1. Therefore, there will be no frequencies due to the light intensity in the solution and the cycles caused by the predator-prey model and their frequencies can be studied.

The factors β and λ are set to $\frac{1}{3*3600*24}\text{s}^{-1}$, the same as used by Steele and Henderson, but rescaled to seconds. The half saturation value $\mu = 1$ mg/m^3, saturation value $c = 10$ mg/m^3 and converting factor $\alpha = 0.5$ are also copied from Steele and Henderson [26]. The mortality factor a is set to $\frac{0.5}{3*3600*24}\text{s}^{-1}$.

For simplicity in the predator-prey equations $m = 1$ and $n = 1$ are chosen. The code is written in such a way that m and n can be easily changed. For brevity, it is chosen to focus on only one model.

Parameter	Notation	Value
Light intensity	$I(t)$	1
Factor $f(P)$	β	$\frac{1}{3*3600*24}$ 1/s
Factor $g(P)$	λ	$\frac{1}{3*3600*24}$ 1/s
Half-saturation value	μ	1 mg/m^3
Saturation value	c	10 mg/m^3
Converting factor	α	0.5
Mortality factor	a	$\frac{0.5}{3*3600*24}$ 1/s
Degree in $g(P)$	n	1
Degree in $h(Z)$	m	1
Length coast	L	500 km
Width coastal area	H	5 km
Depth ocean	$h(x,y)$	linearly from 5 to 50 m
Number of grid points x	N_x	200
Number of grid points y	N_y	80
Number of time steps	T	5000
Time step	dt	20000 s
Boundary condition P left	P_{left}	8.75 mg/m^3
Boundary condition P right	P_{right}	4.375 mg/m^3
Boundary condition P ocean	P_{ocean}	1.75 mg/m^3
Boundary condition Z left	Z_{left}	1.2 mg/m^3
Boundary condition Z right	Z_{right}	3.0 mg/m^3
Boundary condition Z ocean	Z_{ocean}	2.3 mg/m^3
Initial condition P	P_i	7 mg/m^3
Initial condition Z	Z_i	2.4 mg/m^3
Velocity current	$v(x,y)$	varied, realistic 0.03-0.28 m/s
Diffusion coefficient	$D(x,y)$	varied, realistic 1-2000 m^2/s

Table 3.1: Parameters and their value used in the model.

3.3.1. Portuguese west coast as inspiration

The length and width of the coastal area are inspired by the west coast of Portugal. This coast is almost straight and prominently features cliffs, therefore the model is fairly representative.

The length of the west coast of Portugal is approximately 500 km. The considered coastal area is taken to be 5 km wide, so the coastal area reaches to 5 km off the coast. In this region, the depth reaches from around 5 to 50 m. The depth of the ocean is simplified by assuming the depth increases linearly over y, having constant value over x for a value of y. The chosen simplification can be justified by looking at the depth profile of the coast as in figure 3.3a. Here, the depth increases more or less linearly from 5 to 50 m in 5 km.

The velocity of the current is varied to study the effect of the ratios between the convection, diffusion and predator-prey terms. The current at the coast of Portugal is parallel to the coast and southwards, as depicted in figure 3.3b. To be able to use a positive velocity, the domain is mirrored. A typical value of the velocity of this current is 0.03-0.28 m/s [3].

The diffusion coefficient is varied as well to study the effect of the ratios between the convection, diffusion and predator-prey terms. In the literature it can be found that the realistic value for the effective diffusion coefficient to represent the dispersion in the ocean is the eddy diffusion coefficient. This eddy diffusion coefficient is between 1 and 2000 m^2/s [17] [1] [4]. The eddy diffusion coefficient can vary a lot over space and time, as a result of certain patterns (swirls or eddies) in the ocean [4]. For simplicity, the diffusion coefficient is taken to be constant in this model.

To determine the boundary and initial conditions for phytoplankton, the NAUPLIUS database is used [23]. In this database the concentration of chlorophyll is determined by satellite images. For the whole study area, these concentrations are shown in figure 3.3c. In the open ocean the concentration of chlorophyll is low, approximately 0.2 mg/m^3. The concentrations on the south and north boundary are displayed in figures 3.3d and 3.3e. The concentration averages are more or less 0.5 and 1 mg/m^3. These values are chosen to represent the concentration at the boundary. The initial condition is chosen to be 0.8 mg/m^3, following from figure 3.3c. However, these values represent the concentration of chlorophyll and have to be converted to the concentra-

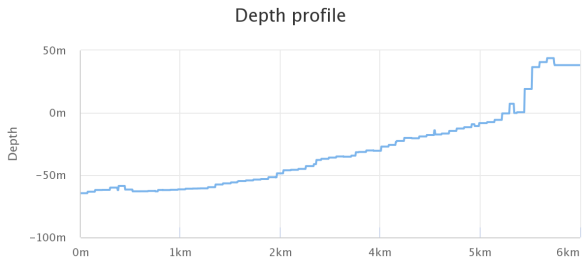

(a) Depth profile of the coastal area near Aljezur [11]

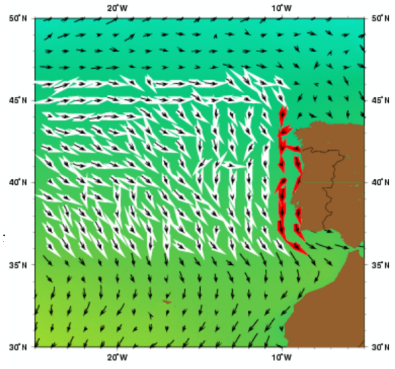

(b) Velocity of the current at the coast of Portugal [3].

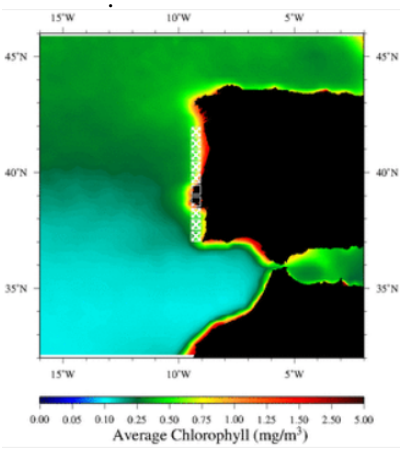

(c) Concentration chlorophyll at the coast of Portugal averaged between 2000 and 2022 [23].

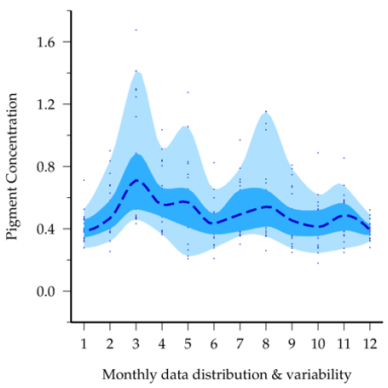

(d) Concentration chlorophyll (mg/m^3) at the right (south) boundary point averaged between 2000 and 2022 [23].

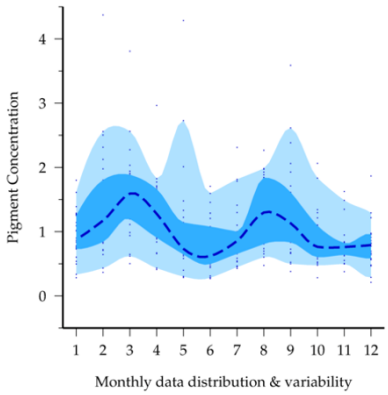

(e) Concentration chlorophyll (mg/m^3) at the left (north) boundary point averaged between 2000 and 2022 [23].

Figure 3.3

tion of phytoplankton expressed in nitrogen (N). The conversion factor equals 8.75 g Chl / g N. This number is determined by the ratio of chlorophyll and N: 1.6 g Chl / mol N [10]. Where 1 mol N equals 14.0067 g. The left, right and ocean boundary condition are set to respectively 8.75, 4.375 and 1.75 mg/m^3, the initial condition to 7 mg/m^3. Notice that the right boundary equals the southern point of the Portuguese west coast, the left boundary equals the northern point. This convention is made such that the velocity in the model is positive.

The value of Z at the boundaries is taken to relate to P by equation 2.13. With the given parameters this renders $Z = (1+P)(1-P/c)$. Note however, that for most a, the solution given by the Steele and Henderson model would have a limit cycle, and therefore Z is actually not equal to the given equation. However, by lack of better information this value has at least a realistic order of magnitude. The left, right and ocean boundary condition are set to respectively 1.2, 3.0 and 2.3 mg/m^3, the initial condition to 2.4 mg/m^3.

3.3.2. Dimensionless numbers

To study the effect of the ratios between the convection, diffusion and predator-prey terms, dimensionless numbers are helpful. These numbers are formed by dividing terms by each other in the equation of the time derivative. All dimensionless numbers related to this model are given in table 3.2. In this table, $m = 1$, $n = 1$ and $I(t) = 1$ are used. For P and Z there is no constant value in the model, therefore the range 0-10 mg/m^3 and 0-6 mg/m^3 are used. For the length scale, for both directions its length is used. Thus for the x-direction L, for the y-direction H. The dimensionless numbers will be used in the analysis to verify the results and to determine the effect of different terms in the model.

In the dimensionless number representing the ratio of diffusion and convection the Péclet number is recognised: Pe $= \frac{vL}{D}$. The dimensionless numbers representing the ratio of convection and predator-prey terms resemble the Damköhler number: Da $= \frac{\text{reaction rate}}{\text{convective mass transport rate}}$. The dimensionless numbers representing the ratio of diffusion and predator-prey terms resemble the second Damköhler number: Da$_{\text{II}}$ =

	Convection	Diffusion x	Diffusion y	Uptake	Grazing	Growth	Mortality
Convection		$\frac{vL}{D}$	$\frac{vH^2}{DL}$	$\frac{v}{\beta(1-\frac{P}{c})L}$	$\frac{v(\mu+P)}{\lambda ZL}$	$\frac{v(\mu+P)}{\alpha\lambda PL}$	$\frac{v}{\alpha aL}$
Diffusion x			$\frac{H^2}{L^2}$	$\frac{D}{\beta(1-\frac{P}{c})L^2}$	$\frac{D(\mu+P)}{\lambda ZL^2}$	$\frac{D(\mu+P)}{\alpha\lambda PL^2}$	$\frac{D}{\alpha aL^2}$
Diffusion y				$\frac{D}{\beta(1-\frac{P}{c})H^2}$	$\frac{D(\mu+P)}{\lambda ZH^2}$	$\frac{D(\mu+P)}{\alpha\lambda PH^2}$	$\frac{D}{\alpha aH^2}$
Uptake					$\frac{\beta(1-\frac{P}{c})(\mu+P)}{\lambda Z}$	$\frac{\beta(1-\frac{P}{c})(\mu+P)}{\alpha\lambda Z}$	$\frac{\beta P(1-\frac{P}{c})}{\alpha aZ}$
Grazing						$\frac{1}{\alpha}$	$\frac{\lambda P}{\alpha a(\mu+P)}$
Growth							$\frac{\lambda P}{a(\mu+P)}$
Mortality							

Table 3.2: Dimensionless numbers corresponding to the equations of the model.

$\frac{\text{reaction rate}}{\text{diffusive mass transport rate}}$.

To analyse the effect of diffusion or convection on the whole predator-prey process, it is better to consider the predator-prey model as one reaction. Of this model the timescale can be determined. Then, for diffusion or convection to influence the solution its timescale should be more or less the same. The timescale of diffusion in the y-direction is given by H^2/D, in the x-direction by L^2/D The timescale of convection in the x-direction is given by L/v.

3.4. Analysis

To analyse the composed model, first the extreme situations are studied; only convection, diffusion or the predator-prey model contribute to the model. These solutions can be compared to a known solution to validate the model. Next, the model is analysed with the terms two by two. Lastly, the complete model is analysed.

3.4.1. Predator-prey model

First of all, the model is evaluated when solely the predator-prey model contributes to the model. This means that $v = 0$ m/s and $D = 0$ m^2/s. There is no current and convection, meaning that each grid point will behave as in the 0D model in chapter 2. Animating the whole study area it can indeed be seen that the solution is uniform. Furthermore, the solution of a grid point is plotted in subplot 3.4a. As comparison, in subplot 3.4b the solution given by the 0D model with the same initial conditions is plotted. The two plots match, therefore the contribution of the predator-prey model is validated.

Furthermore, from these solutions it can be deducted that the predator-prey model has a period of 187.3 days. Thus the predator-prey model has a time scale of $\tau_{pp} = 187.3$ days.

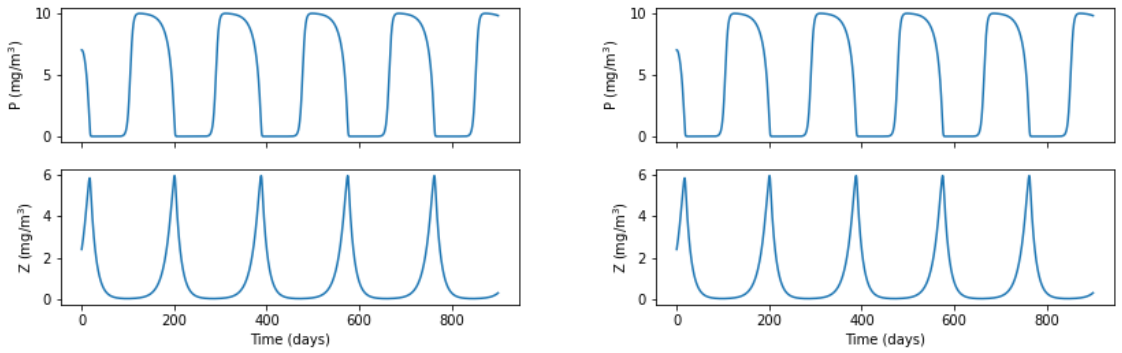

(a) predator-prey model solution following from the 2D model.

(b) predator-prey model solution following from the 0D model.

Figure 3.4

3.4.2. Diffusion

Next, only diffusion is applied in the model. This means $v = 0$ m/s and the predator-prey terms are also multiplied by 0.

The values at the boundaries diffuse into the grid, see figure 3.5a. As the y axis is expressed in 100 m and the x axis in 1 km, the diffusion in the y axis seems to go faster. This is only partially caused by the perspective. Due to the depth that linearly increases, the diffusion in the y term depends on the depth as well. The concentration further of the coast weighs slightly more than the term closer to the coast. Therefore, the diffusion is faster as well.

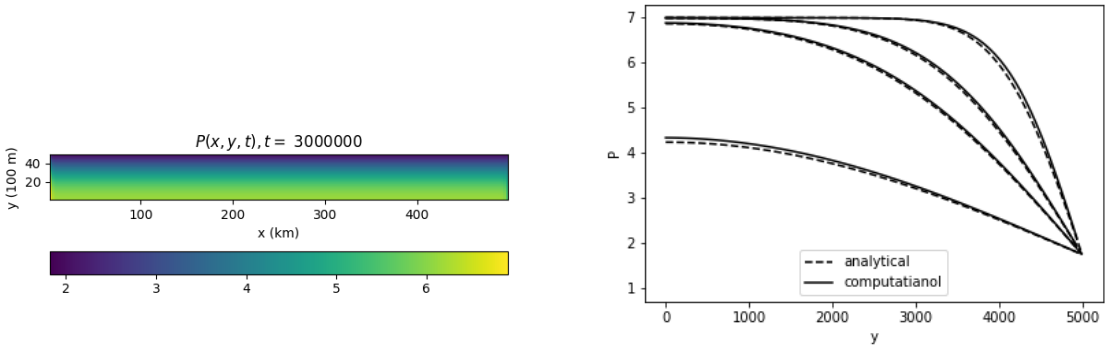

(a) Color coded solution of P over x and y at time $t = 3000000$ s for $D = 1$ m^2/s.

(b) Comparison analytical and computational at different times for $D = 1$ m^2/s.

Figure 3.5

To verify the solution the problem can be solved analytically for constant depth. The derivation of the analytical solution in 2D is given in appendix E.3. The solution is:

$$
\begin{aligned}
P(x,y,t) = &\sum_{n=1}^{\infty} A_n sinh(\tfrac{n\pi(x-L)}{2H}) sin(\tfrac{n\pi y}{2H}) + \sum_{n=1}^{\infty} B_n sinh(\tfrac{n\pi x}{2H}) sin(\tfrac{n\pi y}{2H}) + \sum_{n=1}^{\infty} C_n sinh(\tfrac{n\pi(y-2H)}{L}) sin(\tfrac{n\pi x}{L}) \\
&+ \sum_{n=1}^{\infty} D_n sinh(\tfrac{n\pi(y)}{L}) sin(\tfrac{n\pi x}{L}) + \sum_{n=1}^{\infty} sum_{m=1}^{\infty} E_{mn} sin(\tfrac{n\pi x}{L}) sin(\tfrac{m\pi y}{2H}) e^{-\lambda_{mn}^2 t} \\
A_n &= \tfrac{2}{2Hsin(\frac{-n\pi L}{2H})} \int_0^{2H} P_{left} sin(\tfrac{n\pi y}{2H}) dy \\
B_n &= \tfrac{2}{2Hsin(\frac{n\pi L}{2H})} \int_0^{2H} P_{right} sin(\tfrac{n\pi y}{2H}) dy \\
C_n &= \tfrac{2}{Lsin(\frac{-2n\pi H}{L})} \int_0^{L} P_{ocean} sin(\tfrac{n\pi x}{L}) dx \\
D_n &= \tfrac{2}{Lsin(\frac{2n\pi H}{L})} \int_0^{L} P_{ocean} sin(\tfrac{n\pi x}{L}) dx \\
E_{mn} &= \tfrac{2}{HL} \int_0^{L} \int_0^{2H} [P_i - P_E(x,y)] sin(\tfrac{n\pi x}{L}) sin(\tfrac{m\pi y}{2H}) dy dx \\
\lambda_{mn} &= \sqrt{D} \sqrt{(\tfrac{n\pi}{L})^2 + (\tfrac{m\pi}{2H})^2}
\end{aligned}
\tag{3.38}
$$

This solution is hard to check, due to the integral in E_{mn} in which $P_E(x,y)$ is integrated. As the diffusion in the y-direction is dominant, the 1D diffusion problem is checked in the y-direction. In this solution again the depth is constant. The analytical solution, derived in appendix E.2, is given by:

$$
\begin{aligned}
P(x,t) &= P_{ocean} + \sum_{n=1}^{\infty} a_n sin(\tfrac{n\pi y}{2H}) e^{-D(\frac{n\pi}{2H})^2 t} \\
a_n &= \tfrac{1}{H} \int_0^{2H} [P_i - P_{ocean}] sin(\tfrac{n\pi y}{2H}) dy
\end{aligned}
\tag{3.39}
$$

This solution can be compared to the middle column of the model with constant depth, as the diffusion in the x-direction does not influence the solution here. The analytical and computational solution are plotted for $D = 1$ m^2/s at multiple times in figure 3.5b. Here, it can be seen that the analytical and computational are similar. However, the computational solution is slightly higher than the analytical solution. Testing the sensitivity of the numerical solution, it follows that the error becomes bigger for a larger D. This can be explained as the spatial differentiation error is multiplied by D. The spatial differentiation error can decreased by decreasing the grid size. Furthermore, the time differentiation error can be decreased by decreasing the time step.

3.4.3. Convection

The last extreme situation that is tested is the one where the model only experiences convection. This means that the predator-prey terms are multiplied by 0. Furthermore, there should be no diffusion; $D = 0$ m^2/s. This would lead to the following equation:

$$\frac{\partial P}{\partial t} = -v\frac{\partial P}{\partial x} \tag{3.40}$$

This is a first order equation and therefore only has one boundary condition. Because the 2D model has two boundary conditions, it would be incorrectly posed. The left boundary should be free to flow to the right boundary value, however the right boundary is set to a constant. To solve this problem, a little bit of diffusion is allowed; $D = 10^{-10}$. The analytical solution to equation 3.40 is given in appendix E.1 and is:

$$P(x,t) = \begin{cases} P_{left} & \text{if } x \leq vt \\ P_i & \text{if } x > vt \end{cases} \tag{3.41}$$

Due to the velocity, the left boundary is expected to reach point x at time $t = x/v$. This is the characteristic line. In figure 3.6a t is plotted over x with the values of P color coded. The red line in the figure represents the characteristic line. The figure and the characteristic line agree. However, it is noticeable that the color representing plankton spreads around the line.

In figure 3.6b a plot of the phytoplankton over x is made for different times, again the spread can be seen. The higher the time, the more spread is visible, this agrees with the spread in figure 3.6a. This spread is caused by the numerical approximation in the model. Due to this, the computational solution differs significantly from the analytical solution. This artifact is called numerical diffusion [15].

The numerical diffusion is caused by the chosen differentiation method: backward differentiation. This is a first-order finite difference approximation of the spatial derivative $\frac{\partial P}{\partial x}$. Using the Taylor series expansion for P_{i+1}, the first derivative can be written as:

$$\frac{\partial P}{\partial x} = \frac{P(x_i) - P(x_{i-1})}{\Delta x} - \frac{1}{2}\frac{\partial^2 P}{\partial x^2}\Delta x + \text{higher order terms} \tag{3.42}$$

The higher terms are much smaller than the second derivative and are therefore ignored. In equation 3.40 this gives:

$$\frac{\partial P}{\partial t} = -v(\frac{P(x_i) - P(x_{i-1})}{\Delta x}) + D_{num}\frac{\partial^2 P}{\partial x^2} \tag{3.43}$$

Here $D_{num} = \frac{1}{2}v\Delta x$ is the diffusion coefficient due to numerical diffusion. The numerical diffusion can be reduced by using another differentiation method. However, when using for example the central difference method, solutions with large Péclet number would become unstable. Furthermore, using backward differentiation the error due to numerical diffusion decreases with smaller grid size. In addition, the error increases for larger v. This can be deduced from the substitution in equation 3.40. Lastly, the error decreases with smaller time steps, as then the time integration is more accurate. Testing this in the model, indeed shows the expected changes in the error. Therefore, the model can be validated and the numerical diffusion coefficient can be determined. Moreover, the equilibrium solution which is important for the final density of plankton is not influenced by the numerical diffusion.

3.4.4. Convection and diffusion

With help of the dimensionless numbers it can be determined for which ratio between D and v the diffusion and convection should more or less have the same impact. To determine this the dimensionless number of the diffusion in the y-direction and the convection is used, as the y-direction has the greater diffusion. Then $\frac{vH^2}{DL} = 1$. This results in $D/v = 50$ m. With this ratio, the solution will converge to a solution as depicted in figure 3.7a for $D = 1$ m^2/s and $v = 0.02$ m/s.

The combination of convection and diffusion in the model can be tested by comparing it to the 1D analytical solution given below. To be able to solve the equation analytically the right boundary condition is set at $x \to \infty$. The derivation of this solution is given in appendix E.4.

$$P(x,t) = P_i + \frac{P_{left} - P_i}{2}(erfc(\frac{x - vt}{2\sqrt{Dt}}) + e^{\frac{vx}{D}}erfc(\frac{x + vt}{2\sqrt{Dt}})) \tag{3.44}$$

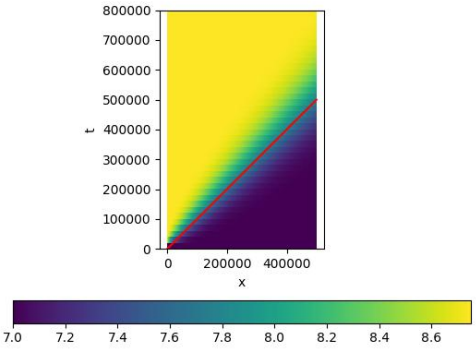

(a) Color coded solution of P over x and t for $v = 1$ m/s. In red the characteristic line corresponding to $v = 1$ m/s.

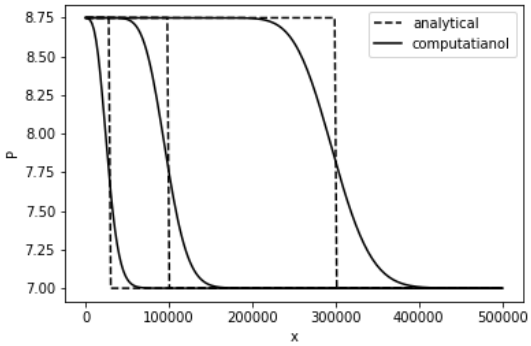

(b) Comparison analytical and computational at multiple times for $v = 0.1$.

Figure 3.6

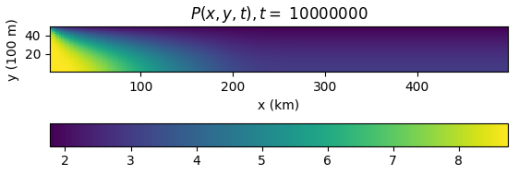

(a) Color coded solution of P over x and y at time $t = 10000000$ s for $D = 1$ m^2/s and $v = 0.02$ m/s.

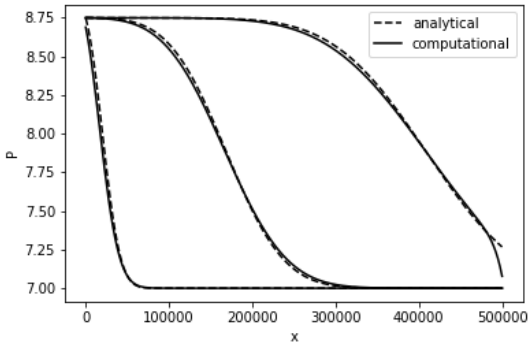

(b) Comparison analytical and computational at multiple times for $D = 200$ m^2/s and $v = 0.02$ m/s.

Figure 3.7

Here $erfc$ is the complementary error function, which is given by $erfc(x) = \frac{2}{\sqrt{\pi}} \int_x^\infty e^{-t^2} dt$. To test the model to this solution, in the model, the upper boundary is set to $\frac{\partial P}{\partial y} = 0$ and the depth is set to a constant. This way, there are no longer differences in the y-direction and therefore the model equals the 1D problem. Furthermore the analytical solution does not take the right boundary into account. Therefore this boundary is set to the initial condition in the model.

In section 3.4.3 it was derived that the numerical diffusion corresponding to the convection has size $D_{num} = \frac{1}{2} v \Delta x = 1250|v|$ m^2/s. Thus, for this numerical diffusion to be neglectable in comparison to the diffusion it should hold that $D >> D_{num}$.

For $v = 0.02$ and $D = 200$, this is the case. In figure 3.7b the analytical and computational solution for $v = 0.02$ m/s and $D = 200$ m^2/s are plotted. The lines corresponding to the solutions match. Only near the right boundary condition a deviation can be seen. In the analytical solution this boundary condition is set at $x \to \infty$ and therefore has no influence.

For smaller values of D the D_{num} contributes relatively more, therefore a larger deviation between the analytical and computational solution can be seen. This deviation decreases for smaller time step and grid size, as then the numerical approximations are more accurate. For small values of D in combination with v the solution could not be checked to the analytical solution, as the analytical solution could not be computed due to limited resources. The exponent $e^{\frac{vx}{D}}$ becomes too large to compute with the available resources.

3.4.5. Diffusion and predator-prey model

With help of the dimensionless numbers an expected value for the diffusion coefficient at which both diffusion and the predator-prey model are important can be found. By setting the dimensionless numbers corresponding to a predator-prey term and the y diffusion term in table 3.2 to 1, the found value for D is between 10 and 45 m^2/s.

With help of the timescales, an expected value for the diffusion coefficient at which both diffusion and the predator-prey model are important can be found as well. This occurs when the ratio of the timescales equals 1. It follows that $D = H^2/\tau_{pp} \approx 1.5\ m^2/s$. This estimate is better as it compares the combination of the predator term as a whole to the diffusion instead of term by term.

To show which effect the diffusion has on the predator-prey model, the minimum and maximum value of P are plotted over y at x=250 km. As the y diffusion is dominant, this gives insight in the solution. The maximum and minimum values are deducted from a period of time in which the solution has converged to its equilibrium solution; either a limit cycle or a constant value. If the P_{max} and P_{min} overlap, the equilibrium is a constant value, otherwise it is a limit cycle. The distance between P_{max} and P_{min} at a certain y value gives the range of the limit cycle at that y value. This is plotted in figure 3.8a for $D = 1\ m^2/s$. Here it can be clearly seen that the range of the limit cycle, which was 0 to 10 mg/m^3 in the 0D model, is reduced over the y axis. This can be explained by the fact that the diffusion suppresses the cycle. This effect is visualised in appendix F.1. The diffusion mixes the concentrations due to which the predator-prey model has no time to develop before it is mixed again. The stronger the diffusion, the stronger the suppression is, until diffusion has the upper hand and the resulting solution is a constant. This relation is displayed in figure 3.8b. The switch to a constant solution is around $D = 2.3\ m^2/s$ in the middle of the grid. For $D > 2.5\ m^2/s$ the solution is constant on the whole grid. This is in fair agreement with the critical $D = 1.5\ m^2/s$ estimated from the time scale analysis.

The realistic value of D between 1 and 2000 m^2/s contains this computed critical value. Therefore, depending on the diffusion coefficient the diffusion has large effect on the solution. The diffusion can mute the predator-prey model slightly or completely take over the solution with the boundary condition P_{ocean}.

In addition to muting the limit cycle, due to diffusion the oscillation frequency of the cycle increases [2]. This is indeed noticeable in the solutions. The muting is however way more important for the quantity of phytoplankton than the frequency. Due to the muting, the average quantity of phytoplankton will decrease. For a very large diffusion coefficient the average will converge to the boundary condition P_{ocean}.

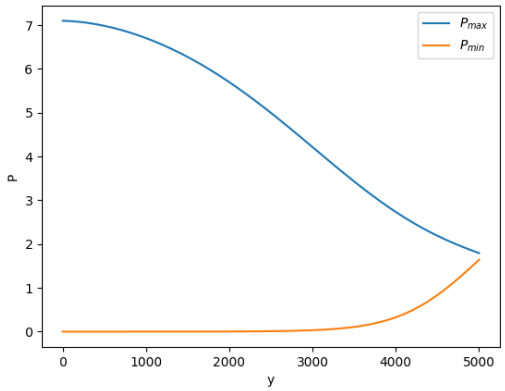

(a) Maximum and minimum of P (mg/m^3) over y (m) at $x = 250$ km for $D = 1$ m^2/s.

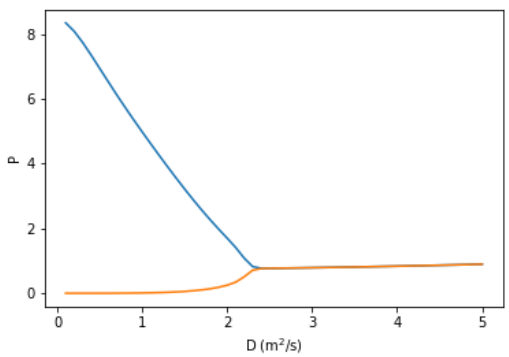

(b) Maximal and minimal value of P (mg/m^3) at $y = 2.5$ km and $x = 250$ km over time when the solution has converged to an equilibrium, plotted over D.

Figure 3.8

3.4.6. Convection and predator-prey model

With help of the dimensionless numbers an expected value for velocity at which both convection and the predator-prey model are important can be found. By setting the dimensionless numbers corresponding to a predator-prey term and the convection term in table 3.2 to 1, the found value for v is between 0.1 and 0.9 m^2/s.

With help of the timescales, an expected value for the velocity at which both convection and the predator-prey model are important can be found as well. This occurs when the ratio of the timescales equals 1. It follows

that $v = L/\tau_{pp} \approx 0.03$ m/s. This estimate is better as it compares the combination of the predator term as a whole to the convection instead of term by term.

To show what effect the convection has on the predator-prey model, a plot of x over t is shown in figure 3.9a with $v = 0.01$ m/s. The solutions of a row in the domain at increasing time are stacked on each other. Here the expected characteristic line is plotted as well (red line). The triangle below the characteristic line has a repeating pattern. This is the predator-prey model acting on the initial condition. Therefore, P fluctuates over time. The triangle above the characteristic line has a repeating pattern as well. However, here P fluctuates in the x-direction. This fluctuation is again caused by the predator-prey model. But this time it is acting on the left boundary condition. In figure 3.9a it can be seen that each point goes to steady state, where the steady state solution is caused by the pattern due to the left boundary condition. Moreover, the red line is not exactly on the switch: it is a little below it. Looking closer to the plot, a spread similarly to the spread in 3.6a can be seen. This spread is caused by the numerical diffusion. As the equilibrium solution is wanted to determine the final density of the phytoplankton, this error is not disastrous.

The left boundary condition flows to the right in the domain while the predator-prey model is acting on it. The lower the velocity is, the more oscillations caused by the predator-prey model fit in the domain. Thus the shorter the wavelength is in the x-direction. This wavelength is expected to relate linear to the velocity. At a certain velocity the boundary condition flows so fast through the domain that the predator-prey model has had little time to develop before it reaches the right boundary. Then, the left boundary condition will dominate the solution. This effect is visualised in appendix F.2.

The change in wavelength in the x-direction due to the velocity is displayed in figure 3.9b. Here the expected linear relation is observed. For small velocities there is a small deviation, this can be explained by the fact that at the final time of the simulation the associated solution had not reached its equilibrium solution. Therefore, the measurement is less accurate. For larger values of v, the wavelength goes to zero, as there are no longer two peaks in the equilibrium solution from which the wavelength can be deducted. This occurs at $v > 0.025$ m/s, in fair agreement with the critical value $v = 0.03$ m/s estimated from the time scales.

To study the effect of convection on the biomass of phytoplankton, the average concentration of phytoplankton in the domain is computed for a range of velocities. This is displayed in figure 3.9c. Here the following can be seen: for small velocities figure 3.9a applies. Moving up to higher velocities until $v = 0.04$ m/s, less waves fit in the domain causing to sometimes partially lose the last peak of P. This causes the fluctuations on the left of figure 3.9c. The amplitude of these fluctuations lower for lower velocities, as then the broad of the peaks that can be partially lost is smaller. Between $v = 0.04$ m/s and $v = 0.06$ m/s only the first peak in figure 3.9a is still in the domain. By increasing the velocity only part of this peak is still in the domain, causing the almost linear decrease in figure 3.9c. From $v = 0.06$ m/s on, the peak right next to the boundary starts to play a bigger role, causing the increase in 3.9c.

The observed pattern is caused by the left boundary condition. However, the value of the boundary does not matter for v smaller than 0.06 m/s, as the limit cycle that forms in that case does not depend on the initial condition, here the left boundary condition. However, for v larger than 0.06 m/s the chosen boundary condition is important, as then the convection suppresses the predator-prey terms. The realistic value of $v =$ 0.03-0.28 m/s contains both of these situations.

3.4.7. Convection, diffusion and predator-prey model

To see a combination of convection, diffusion and predator-prey, all three terms should contribute equally to the model. This can be determined by the timescales. As seen in the previous sections $D/v \approx 50$ m, $D \approx 1.5$ m/s^2 and $v \approx 0.03$ m/s. It can be noticed that this D and v have the ratio $D/v \approx 50$ m.

For $D = 1$ m^2/s and $v = 0.02$ m/s, the solution after some time is plotted in figure 3.10a. This is as expected by the separate analysis of convection and diffusion in combination with the predator-prey model: due to convection the fluctuation pattern in the x-direction appears, due to diffusion the solution is muted in the y-direction. This effect is visualised in appendix F.3.

To investigate what happens at different ratios of D and v multiple plots are made to display the solutions. These plots display a value in color code corresponding to a combination of D and v. First of all, in figure 3.11a the wavelength in the x-direction is plotted over D and v. As learned from the analysis solely with convection and the predator-prey model, the wavelength increases with increasing velocity, until there are no longer two peaks in the x domain and the wavelength cannot be measured. Noticeable is that the wavelength does indeed increase with increasing velocity and at a certain moment cannot be measured anymore. The bottom row ($D = 0.1$ m^2/s) of figure 3.11a agrees with figure 3.9b. Furthermore, it can be seen that the wavelength decreases for a higher diffusion coefficient. As the wavelength decreases, for larger velocities the second peak can be

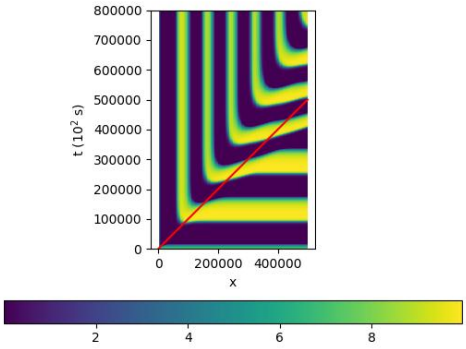

(a) Color coded solution of P over x and t for $v = 0.01$ m/s. In red the characteristic line corresponding to $v = 0.01$ m/s.

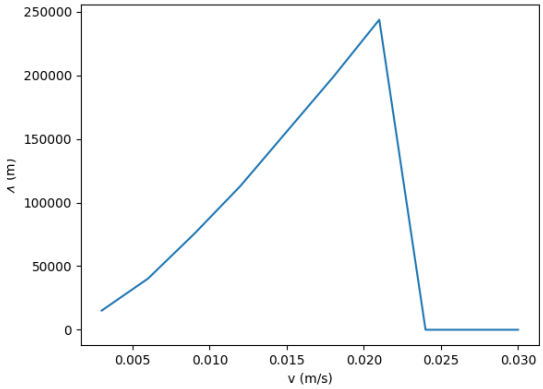

(b) Wavelength in the x-direction plotted over v.

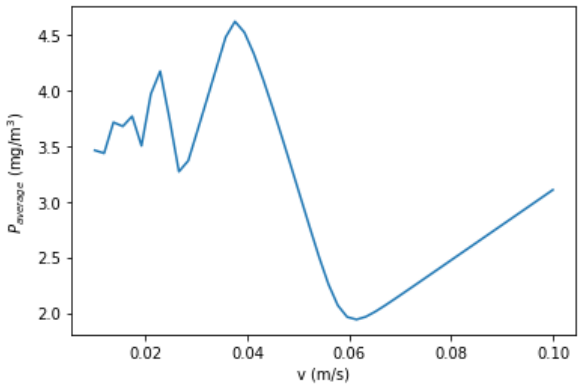

(c) Average value of phytoplankton plotted over v.

Figure 3.9

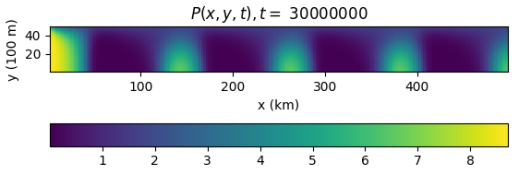

(a) Color coded solution of P over x and y at time $t = 30000000$ s for $D = 1$ m^2/s and $v = 0.02$ m/s.

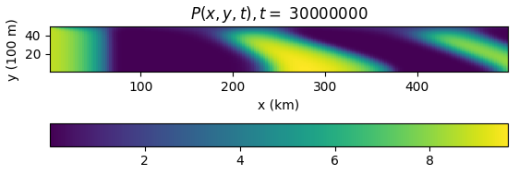

(b) Color coded solution of P over x and y at time $t = 30000000$ s for $D = 0.1$ m^2/s and $v = 0.03$ m/s.

Figure 3.10

found in the domain as well. Therefore, the wavelength can be measured again.

In figure 3.11b, the diffusion is plotted at a peak of the fluctuations in the x-direction. At the middle of the y-direction, the P value is displayed. The expectation after the analysis solely with diffusion and the predator-prey model is that this value decreases for higher D; the more diffusion, the more important the boundary condition P_{ocean} which is relatively low. This trend is indeed detected. Furthermore, it is noticed that the

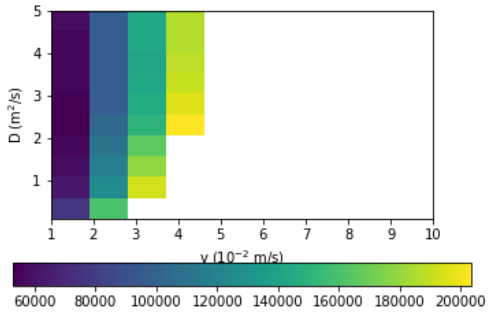

(a) Color coded wavelength in the x-direction over D and v.

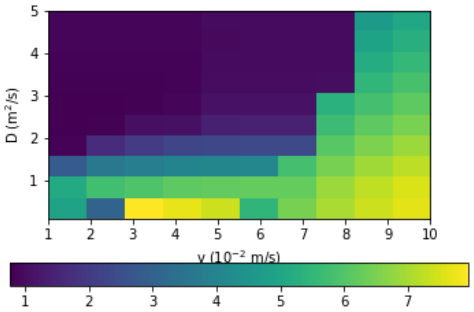

(b) Color coded diffusion over D and v. Displayed by plotting the value of P at $y = 2.5$ km corresponding to the x in which at y=0 km a peak of P is measured.

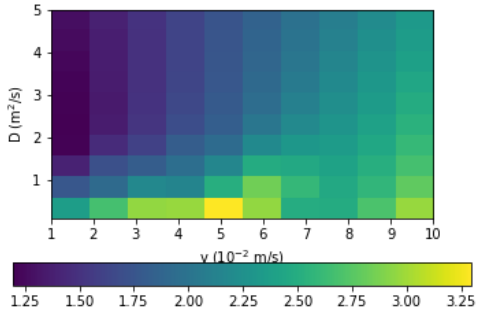

(c) Color coded average P of the domain over D and v.

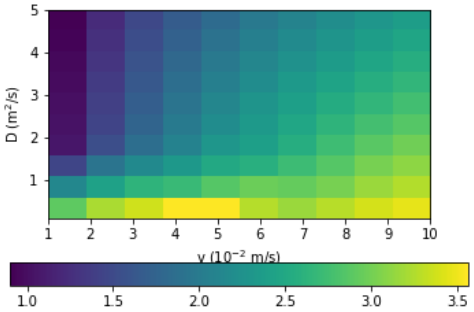

(d) Color coded standard deviation of P of the domain over D and v.

Figure 3.11

value becomes higher for larger velocity. This can be explained by the fact that if the velocity is higher, the left boundary condition takes over, which has a relatively high value. The bottom row ($D = 0.1$ m^2/s) in figure 3.11b deviates from the two previously described trends. Here $D/v < 50$, which means that convection has a larger effect in the model than diffusion. Such a situation leads to skewed patterns as displayed in figure 3.10b. As the peaks are measured in the bottom row of the grid, at this x value the impact of the diffusion in the y-direction is measured. Due to the skewed pattern, this measurement is tricky and therefore the bottom row has a different pattern.

Next, in figure 3.11c, the average value of P over the domain is plotted over D and v. As for all v, and therefore for all D in combination with convection the solution converges to a steady state solution, the solution is integrated over space and divided by the total space. The result is the average P of the solution. Due to the convection in the bottom row having more impact than the relatively low diffusion, the average P is similar to figure 3.9c. Furthermore, it is noticed that the higher the diffusion the lower the average, as the relatively low boundary condition P_{ocean} has more impact. On the other hand, for high velocity the relatively high boundary condition has more impact, thus the average of P increases.

Lastly, in figure 3.11d, the standard deviation of the solution is displayed over D and v. The standard deviation of the lexicographic vector representing the solution gives insight in the average variability of the function. The higher the diffusion, the more the solution is influenced by the constant boundary value, lowering variability and thus the standard deviation.

In conclusion, the effects of the diffusion and convection are combined. The model experiences both diffusion and convection more or less equally when the Péclet number $\frac{vH^2}{DL} \approx 1$, resulting in $\frac{D}{v} \approx 50$ m. If this number is significantly larger than 50 m, diffusion dominates the solution. If the number is significantly smaller than 50 m, convection dominates the solution.

4

Temperature rising

Due to climate change, the temperature of the ocean is rising [5]. This temperature increase is depicted in figure 4.1. The rising temperature effects the growth of plankton. This dependency is described in section 4.1. Afterwards, the effect of the dependency on the 0D and 2D model is analysed.

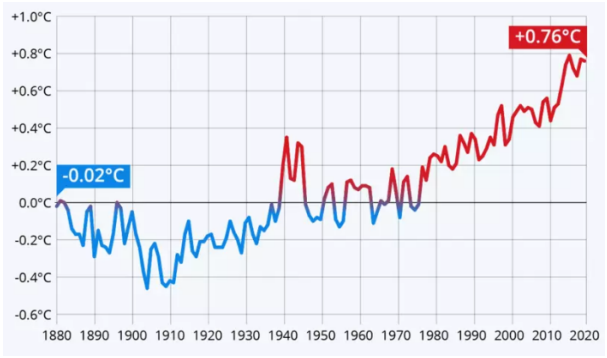

Figure 4.1: Sea temperature rising [5].

Next to the rising temperature due to climate change, the temperature of the water also depends on the location. In figure 4.2a one can see that the average temperature of the water in the chosen domain is higher in the south than in the north. From figure 4.2b and 4.2c, it can be seen that the average temperature ranges from more or less 16 to 18 °C. Furthermore, the temperature depends on the season. The pattern is similar to a sinus with the period of a year and an amplitude of 2 °C around the mean temperature. These fluctuations in temperature impact the plankton population as well.

4.1. Temperature dependence growth phytoplankton

The optimum temperature is different for all plankton species, corresponding to different growth rate curves [13]. The plankton population in the chosen domain consists of many plankton species. It is complex to model all species separately. As a solution, for the given temperature the growth rate is taken to equal the maximum growth rate corresponding to this temperature. This corresponds to a line through the maxima of the separate growth rate curves. This estimation is based on the idea that plankton migrates to where circumstances are optimal. Thus, at a certain temperature the species for which the temperature is optimal dominates. This estimation is represented by the Eppley curve [12], as shown in figure 4.3. The formula for the Eppley curve is:

$$\beta_{Eppley} = 10^{0.0275T - 0.07} \tag{4.1}$$

Here the temperature T is given in °C. β_{Eppley} replaces the β previously used in the model. β_{Eppley} gives the growth rate per day. By dividing by 24h/d·3600s/h this is rescaled to a time scale of 1 second.

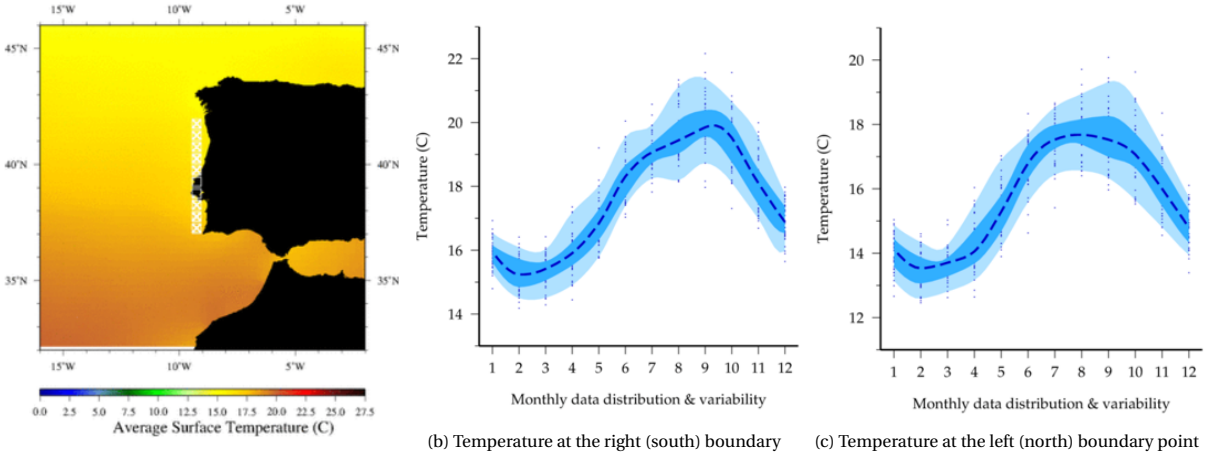

(a) Temperature at the coast of Portugal [23].

(b) Temperature at the right (south) boundary point [23].

(c) Temperature at the left (north) boundary point [23].

Figure 4.2

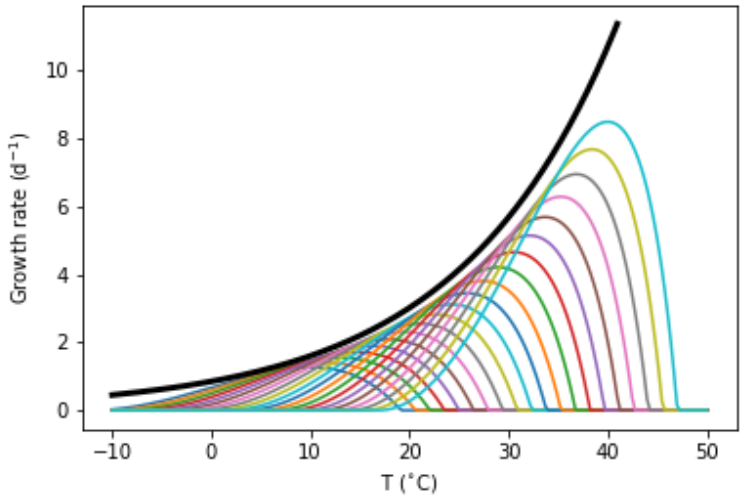

Figure 4.3: Growth rate of phytoplankton corresponding to multiple optimal temperatures in different colors with the Eppley curve in black.

4.2. Steele and Henderson

Analysing the effect of the temperature change in the Steele and Henderson model it is noticeable that only the period of the fluctuations changes in time. This change in period is displayed in figure 4.4a. This change can be explained by the following. The higher β is due to temperature, the higher the growth term is. However, the concentration phytoplankton has a maximum level, given by the saturation factor c, which cannot be exceeded. Therefore this change is not seen in the amplitude of the fluctuations. As the growth is faster, the growth will start again sooner. But as the grazing is dependent on the concentration of phytoplankton, the grazing will start sooner as well. This way the smaller period can be explained.

Due to the higher growth term the model is unstable for the previous used time step $dt = 20000$ s. Therefore, the time step is changed to $dt = 2000$ s. When the temperature is included in the 0D model, the time scale decreases from $\tau_{pp} = 107$ s to $\tau_{pp} = 98$ s with increasing temperature.

Due to the higher frequency in time, the average P in time increases. The same amount of phytoplankton occurs in a shorter period of time. This has the relation $P_{tot,1period}/T$. Thus a $\sim 1/T$ relation. This is displayed in figure 4.4b

Including the fluctuations of the temperature in time, the temperature is given by a sinus with the period of a year and an amplitude of 2 °C around the mean temperature. Due to this fluctuation the period of the

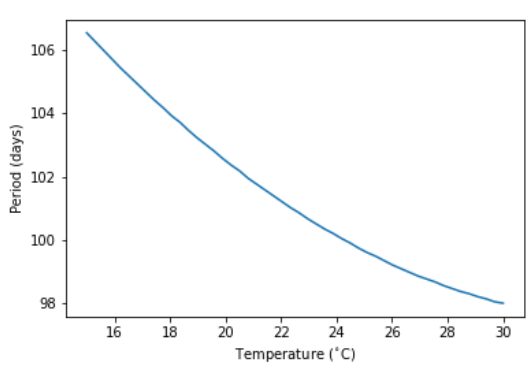

(a) Period of the predator-prey model over temperature.

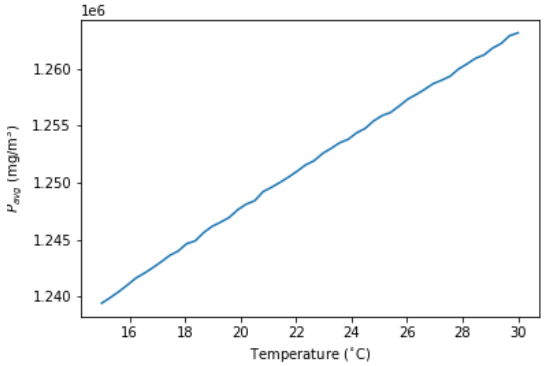

(b) Average P in time over temperature.

Figure 4.4

predator-prey model would fluctuate as well, with a period corresponding to the temperature $\pm 2\,^{\circ}$C. According to figure 4.4a this would cause a fluctuation in the period with an amplitude smaller than 2 days. Therefore, it is a good estimation to take the timescale equal to the timescale with constant temperature.

4.3. 2D model

The change in period of the predator-prey model means that there is also a change in the timescale corresponding to the predator-prey model, τ_{pp}. The ideal ratio is still $\frac{D}{v} = 50$ m. However, $D = H^2/\tau_{pp}$ and $v = L/\tau_{pp}$ do change due to the timescale. This D and v corresponding to each temperature are plotted in figure 4.5a and 4.5b. As the timescale is equal to the period, the timescale is decreasing for increasing temperature. And as D and v are related to τ_{pp} with $\sim 1/\tau_{pp}$, the expected values where all terms have an impact are higher. This means that for higher temperature the predator-prey term has a bigger impact. However, this change in D and v is relatively small in comparison to the range of the realistic values. Therefore, it can be deducted that the temperature is not very important in the model.

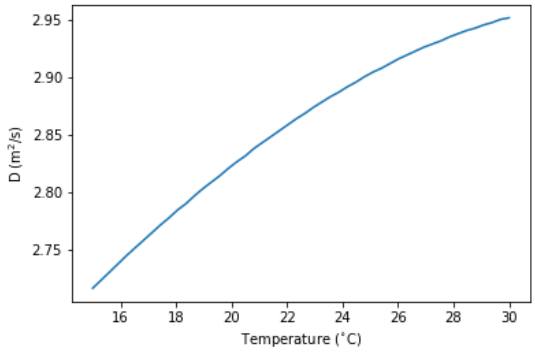

(a) Critical diffusion value over temperature.

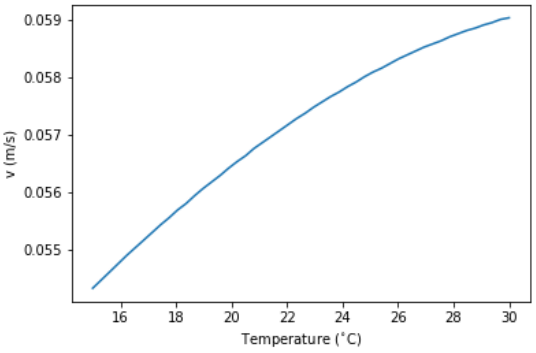

(b) Critical velocity value over temperatures.

Figure 4.5

Furthermore, due to the temperature dependence on location the predator-prey model has a slightly bigger impact in the north than in the south.

5

Discussion

In this report a lot of assumptions have been made to simplify a real life situation. In addition parameters are set, and grid sizes are chosen. All these choices and simplifications have a reason, however they are arguable.

5.1. Numerical model

First of all, the presented model has to be solved numerically as it is too complex to solve analytically. For solving numerically, a grid size and time step have to be chosen. The smaller these steps are chosen, the more accurate the solution is. However due to the running time of the model and limited resources the grid size and time step are set to the chosen values. Specifically, the time step is chosen to be small enough, so that the predator-prey model is stable. It would be better to take smaller time steps and smaller grid size to get a more accurate solution. To make this possible in a limited time, the code for the model could be made more efficient.

Next, the formed model is only successfully validated for small values of v with large values of D. This is caused by the numerical diffusion, which depends on time step size, grid size and the value of v and D. The higher these values, the larger the error. For smaller values of D in combination with v the solution could not be checked to the analytical solution, as the analytical solution could not be computed due to limited resources.

5.2. Physical assumptions

Furthermore, a lot of physical assumptions are made to simplify the model. For example, the coastline that is used is considered to be a straight line. In addition, the depth is assumed to increase linearly and it is assumed that everywhere in the depth there is the same amount of phytoplankton. However, this assumption is harsh, as the amount of plankton does depend on the depth. Therefore, in the growth factor the depth should be taken into account. However, this would mean that the model has to be made 3D, which takes more computing time.

Moreover, the velocity v and diffusion coefficient D are set to a constant over the whole region. In real life however, the velocity and diffusion coefficient are not constant and static, but very location dependent and dynamic. Taking this into account would lead to a more accurate solution. This effect should be studied in more detail.

Especially the behaviour of the diffusion coefficient has to be studied as location dependent and dynamic. The eddy diffusion coefficient can vary a lot in size over space and time due to certain patterns (swirls or eddies) in the ocean [4]. Such a pattern is displayed in figure 5.1a. In literature, an article is found on the effect of an eddy on the coastal area of Southern California [6], see figure 5.1b. The more in the centre of an eddy, the lower the diffusion coefficient corresponding to it. This makes it possible for the plankton to bloom in the centre of an eddy as shown in figure 5.1c and 5.1d.

In figure 5.1, it is also noticeable that the studied coastal area is only a small part of the region where plankton blooms. To investigate the whole pattern as one, it would therefore be better to study a larger area. However, then some assumptions in this report should be reconsidered.

In addition, the boundary conditions are set to a constant. These constants are gathered from data. However, in the data it can be seen that the value at the boundary fluctuates. Therefore it might be better to take a

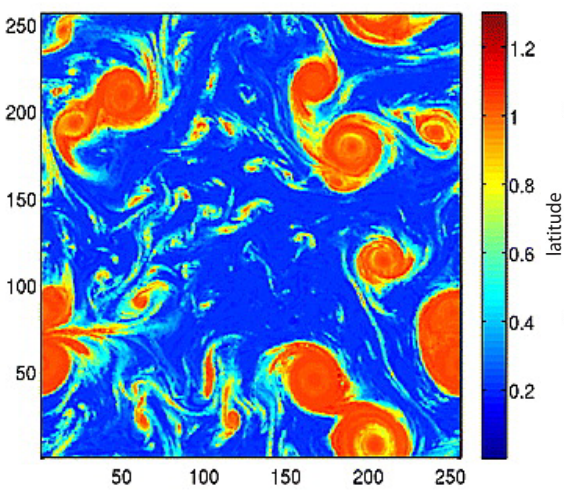

(a) Pattern of phytoplankton in a dynamic model of the ocean [4].

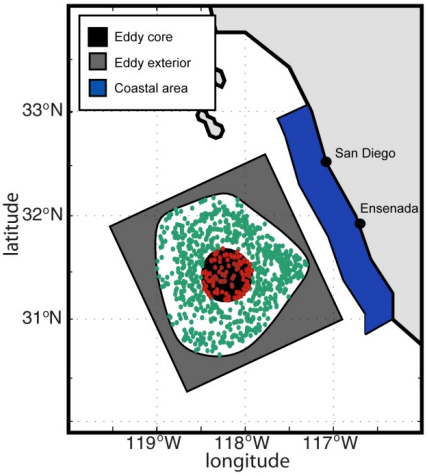

(b) Pattern of an eddy near the coast in Southern California [6].

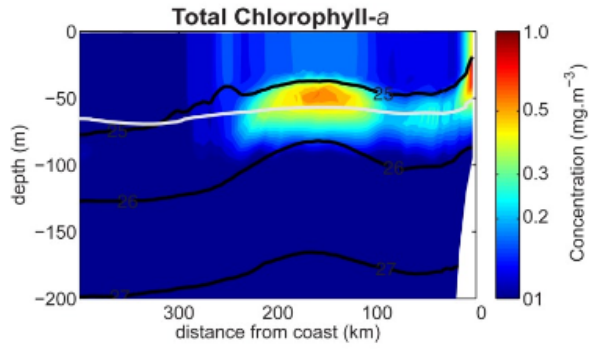

(c) Concentration chlorophyll over the distance from the coast and depth in Southern California [6].

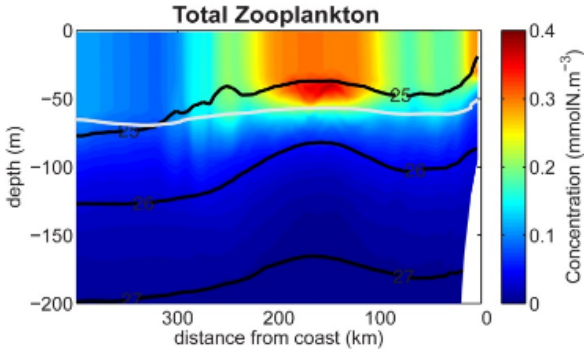

(d) Concentration zooplankton over the distance from the coast and depth in Southern California [6].

Figure 5.1

fluctuating boundary condition in time, for example the 0D limit cycle. Due to convection the left boundary value is important. Up to a certain velocity only the limit cycle corresponding to the chosen parameters matters, this is independent of the boundary condition. For a higher velocity however the value of the boundary condition value takes over. For the diffusion, the boundary condition P_{ocean} takes over for a higher diffusion coefficient.

5.3. Biological assumptions

Another assumption that is made to simplify the model is to set some variables in the Steele and Henderson model to arbitrary values. These values are copied from Steele and Henderson, and simplify the model by reducing the amount of variables. However, by comparing the values of the growth term in chapter 4 to the set parameters by Steele and Henderson, these differ by a factor 10. This causes a change in the model. This could be the case for the other set parameters too. The effect of these parameters should be studied, and values based on more founded literature research should be chosen.

Moreover, to investigate the temperature dependency of the plankton population the Eppley curve is used, which is based on the assumption that the phytoplankton species for which the temperature is optimal is sovereign. This assumption is harsh, as the water holds many different species of phytoplankton. However, it is shown that the phytoplankton migrates to other areas where the temperature is more optimal [28]. It might still be better to make a more moderate approximation.

When taking the temperature rise of the water into account, this is only done in relation to phytoplankton. However the temperature rise can also have an effect on zooplankton. The zooplankton could for example eat relatively more or have a higher mortality. This change would have an impact on the 0D predator-prey model and therefore an influence in the 2D model. This relation between temperature and zooplankton should be

further studied and included in the model.

Lastly, the result found in this report, namely that by increasing temperature the phytoplankton population increases a bit, has a side note. In this model, only the temperature dependence on the growth of phytoplankton is studied. The other impacts of the temperature rise and other impacts of climate change, such as acidification of phytoplankton by the abundance of CO_2, are not considered. Therefore, the result of this report cannot directly be applied to the big picture. Only a specific relation of the temperature effect on the growth of phytoplankton is studied. From data, it follows that the total plankton population is decreasing [18]. To know due to which aspects of climate change this occurs further research is needed. Another side note is that this report is based on assumptions about plankton based on observations of phytoplankton nowadays. However nature changes; it evolves. This means that the behavior of plankton could change.

6

Conclusion

The research question 'Is the temperature increase of the water important for the development in space and time of the plankton population in a 2D model of a coastal area of an ocean?' is answered with help of a simple 2D model of a coastal area. The 2D model includes three mechanisms: convection (v), diffusion (D) and the predator-prey model of Steele and Henderson. This model is validated against analytical solutions for small values of v and D. It can be made more accurate for larger values by using a smaller time step and grid size. Due to limited time and resources, this is left out of scope in this project. To understand the effect of convection and diffusion in the 2D model two sub questions are answered.

First, the following sub question is answered: *is the diffusion important for the development in space and time of the plankton population in a 2D model of a coastal area of an ocean?* The diffusion appears to be dominant in the direction perpendicular to the coast. Due to the diffusion the repeating pattern, or limit cycle, of the predator-prey model is suppressed. Its range gets smaller until the plankton population is completely constant for a diffusion coefficient $D > 2.5$ m^2/s. This critical value is included in the realistic value of D, which varies from 1 to 2000 m^2/s. The formed model with constant diffusion coefficient gives insight in what happens for a certain diffusion coefficient. It shows that the diffusion is important for the development in space and time of the plankton population in the 2D model.

Next, the second sub question is answered: *Is the convection important for the development in space and time of the plankton population in a 2D model of a coastal area of an ocean?* Due to convection, the limit cycle corresponding to the boundary condition occurs in the direction parallel to the coast, making every point in the domain steady state. The higher the velocity v corresponding to the convection is, the less oscillations in phytoplankton density there are in the domain, thus the larger the wavelength of the oscillation is. For $v > 0.06$ m/s the current is so fast that the predator-prey model has little time to develop before it reaches the right boundary, making the left boundary value more important. This critical value is included in the realistic value of v, which varies from 0.03 to 0.28 m/s. Thus, the exact value of the velocity v corresponding to the convection is important for the development of the plankton population in space. As the solution of the formed model reaches a steady state, the development over time is no longer important.

The model experiences both diffusion and convection more or less equally when the Péclet number $\frac{vH^2}{DL} \approx 1$, resulting in $\frac{D}{v} \approx 50$ m. If this number is significantly larger than 50 m, diffusion dominates the solution. If the number is significantly smaller than 50 m, convection dominates the solution.

Now the main question can be answered: *is the temperature increase of the water important for the development in space and time of the plankton population in a 2D model of a coastal area of an ocean?* By increasing the temperature of the water the growth rate of phytoplankton increases. Due to this increase, the timescale of the predator-prey (τ_{pp}) decreases. The value of D and v for which the predator-prey model and diffusion and convection all influence the solution equally depends on the timescale with the factor $1/\tau_{pp}$. A smaller time scale means that the predator-prey model contributes more to the model. However, this change is very small in comparison to the scale of the realistic values. In conclusion, in the formed 2D model the temperature increase of the water is not important for the development in space and time of the plankton population.

The results of this report are influenced by the assumptions and approximations made. For example, the boundary conditions, the diffusion coefficient and velocity are set to a constant and the considered region is rectangular, in which the density of phytoplankton does not depend on the depth. Moreover, only the influence of temperature on phytoplankton is taken into account, not the influence on zooplankton. Thus, in

this study, several processes, both physical and biological, are described with constants and simplifications. Improving the model is left to future studies, and requires much higher resolution simulations and more sophisticated biological and physical models than employed here.

Bibliography

[1] Marine habits. In *Encyclopedia of Microbiology (Third Edition)*, pages 258–277. 2009.

[2] M.R. Adriaens. Plankton populaties in rivieren, analyse van patronen in planktonmodellen voor rivierstructuren. Master's thesis, TU Delft, 2020.

[3] B. Bischof, A.J. Mariano, and E.H. Ryan. The portugal current system. https://oceancurrents.rsmas.miami.edu/atlantic/portugal.html, 2003. accessed May 12, 2022.

[4] A. Bracco, S. Clayton, and C. Pasquero. Horizontal advection, diffusion, and plankton spectra at the sea surface. *Journal of Geophysical Research*, 114(C2), 2009.

[5] K. Buchholz. Climate change: How much is the ocean warming by? https://www.weforum.org/agenda/2021/01/ocean-warming-climate-change-sea-crisis-temperature/, 2021. accessed May 16, 2022.

[6] F. Chentillat, P.J.S. Franks, P. Riviere, X. Capet, N. Grima, and B. Blanke. Plankton dynamics in a cyclonic eddy in the southern california current system. *Journal of Geophysical Research: Oceans*, 120(8):5566–5588, 2015.

[7] National Research Council. *Managing wastewater in coastal utban areas*. The National Academies Press, 1993.

[8] R.C. Daileda. The two dimensional heat equation. http://ramanujan.math.trinity.edu/rdaileda/teach/s12/m3357/lectures/lecture_3_6_short.pdf, 2012. accessed May 25, 2022.

[9] P. Dawnkins. Diiferential equations laplace's equation. https://tutorial.math.lamar.edu/classes/de/laplaceseqn.aspx, 2021. accessed May 25, 2022.

[10] Y. Dijkstra. Conversation with Yoeri Dijkstra.

[11] EMODnet. Emodnet bathymetry viewing and download service. https://portal.emodnet-bathymetry.eu/, 2022. accessed May 12, 2022.

[12] R.W. Eppley. Temperature and phytoplankton growth in the sea. *Fishery Bulletin*, 70(4):1063–1085, 1972.

[13] G.M. Grimaud, V. Le Guennec, S.D. Ayata, F. Mairet, A. Sciandra, and O. Bernard. Modelling the effect of temperature on phytoplankton growth across the global ocean. *IFAC-PapersOnLine*, 48(1):228–233, 2015.

[14] D.K. Jaiswal, A. Kumar, and R.R. Yadav. Analytical solution to the one-dimensional advection-diffusion equation with temporally dependent coefficients. *Journal of Water Resources and Protection*, 3(1):76–84, 2011.

[15] D.P. Karadimou and N.C. Markatos. Study of the numerical diffusion in computational calculations. *Numerical Simulations in Engineering and Science*, 2018.

[16] S.R. Lay. *Analysis with an Introduction to Proof*. Pearson Education, 2013.

[17] R. Lumpkin, A. Treguier, and K. Speer. Lagrangian eddy scales in the northern atlantic ocean. *Journal of Physical Oceanography*, 32(9):2425–2440, 2002.

[18] L. Morello. Phytoplankton population drops 40 percent since 1950. https://www-scientificamerican-com.tudelft.idm.oclc.org/article/phytoplankton-population/#:~:text=Researchers%20at%20Canada's%20Dalhousie%20University,surface%20temperatures%20are%20to%20blame., 2010. accessed June 4, 2022.

[19] R. Morgan. Linearization and stability analysis of nonlinear problems. *Rose-Hulman Undergraduate Mathematics Journal*, 16(2), 2015.

[20] NOAA. What are plankton? https://oceanservice.noaa.gov/facts/plankton.html, 2019. accessed June 2, 2022.

[21] NOAA. Aquatic food webs. https://www.noaa.gov/education/resource-collections/marine-life/aquatic-food-webs#:%7E:text=Phytoplankton%20and%20algae%20form%20the,%2C%20corals%2C%20and%20baleen%20whales., 2019. accessed June 2, 2022.

[22] NOAA. How much oxygen comes from the ocean. https://oceanservice.noaa.gov/facts/ocean-oxygen.html, 2021. accessed June 2, 2022.

[23] T. O'Brien. Nauplius - spatio-temporal exploration and data. https://www.st.nmfs.noaa.gov/nauplius/html/mapmenu-europe.html, 2022. accessed May 12, 2022.

[24] E.B. Ornolfsdottir. Phytoplankton community growth-rate response to nutrient pulses in a shallow turbid estuary, galveston bay, texas. *Journal of Plankton Research*, 26(3):325–339, 2004.

[25] S. Rigby. The ocean captures twice as much carbon dioxide as previously thought. https://www.sciencefocus.com/news/the-ocean-captures-twice-as-much-carbon-dioxide-as-previously-thought/1, 2020. accessed June 2, 2022.

[26] J.H. Steele and E.W. Henderson. The role of predation in plankton models. *Journal of Plankton Research*, 14(1):157–172, 1992.

[27] H. Van den Akker and R. Mudde. *Fysische Transportverschijnselen - denken in balansen.* Delft Academic Press, 2014.

[28] Vroege Vogels. Vroege vogels tv plankton. https://www.bnnvara.nl/vroegevogels/videos/577585, 2022. accessed April 14, 2022.

A

Reducing number of variables

In the model given by Steele and Henderson there are a lot of parameters: nine in total. These parameters are summarised in table A.1. By rewriting the system to a dimensionless form the system can be represented by seven parameters; the number of parameters can be reduced by two. The derivation is given below, here all parameters are separated in its size ($\bar{P}$) and its unit (P^*), making $P = \bar{P}P^*$. This notation makes it possible to rewrite the derivative: $\frac{dP}{dt} = \frac{\bar{P}dP^*}{\bar{t}t^*}$. Now using this notation in equation 2.3 with $I(t) = 1$ and equation 2.5, 2.6 and 2.7, result in:

$$\frac{\bar{P}dP^*}{\bar{t}dt^*} = \bar{\beta}\beta^*\bar{P}dP^*(1 - \frac{\bar{P}P^*}{\bar{\gamma}\gamma^*}) - \frac{\bar{Z}Z^*\bar{\lambda}\lambda^*\bar{P}^nP^{*n}}{\bar{\mu}\mu^* + \bar{P}^nP^{*n}} \tag{A.1}$$

$$\frac{\bar{Z}dZ^*}{\bar{t}dt^*} = \frac{\bar{\alpha}\alpha^*\bar{\lambda}\lambda^*\bar{P}^nP^{*n}\bar{Z}Z^*}{\bar{\mu}\mu^* + \bar{P}^nP^{*n}} - \bar{\alpha}\alpha^*\bar{\delta}\delta^*\bar{Z}^mZ^{*m} \tag{A.2}$$

Rewriting these equations yields:

$$\frac{dP^*}{dt^*} = \bar{\beta}\bar{t}\beta^*dP^* - \frac{\bar{\beta}\bar{P}\bar{t}}{\bar{\gamma}}\frac{\beta^*p^{*2}}{\gamma^*} - \frac{\bar{Z}\bar{\lambda}\bar{P}^{n-1}\bar{t}Z^*\lambda^*P^{*n}}{\bar{\mu}\mu^* + \bar{P}^nP^{*n}} \tag{A.3}$$

$$\frac{dZ^*}{dt^*} = \frac{\bar{\alpha}\bar{\lambda}\bar{P}^n\bar{t}\alpha^*\lambda^*P^{*n}Z^*}{\bar{\mu}\mu^* + \bar{P}^nP^{*n}} - \bar{\alpha}\bar{\delta}\bar{Z}^{m-1}\bar{t}\alpha^*\delta^*Z^{*m} \tag{A.4}$$

The parameters of this dimensionless system are notated in table A.1. Some are simplified, by dividing by other parameters.

Steele and Henderson	**Dimensionless system**
P	P
Z	βt
t	γ
α	$Z\lambda t$
β	μ
γ	$\alpha\lambda t$
δ	$\alpha\delta Z^{m-1}t$
λ	
μ	

Table A.1

The minimal number of parameters can be determined by the Buckingham Pi theorem. This theorem states that the number of dimensionless variables is given by the number of variables in the system minus the number of fundamental dimensions. To determine the number of dimensionless variables this way, it is needed to write down the units of the parameters:

- $\gamma, P, Z : \mathrm{mg/m^3}$
- $\beta, \lambda : 1/\mathrm{s}$
- $\mu : (\mathrm{mg/m^3})^n$
- $\delta : (\mathrm{mg/m^3})^{m-1}/\mathrm{s}$

The units contain three fundamental dimension, however $\mathrm{mg/m^3}$ always appears in this form; mg and m do not appear separately, therefore this is taken as one fundamental dimension. The Buckingham Pi theorem then yields that there are seven dimensionless variables as well, supporting the found dimensionless system.

B

Derivation convection and diffusion

In this appendix the mass balance corresponding to a grid cell is rewritten t a simpler system of equations. The mass balance is given by:

$$\begin{aligned}\frac{\partial}{\partial t}(\int_x^{x+dx}\int_y^{y+dy} h(x,y)c(x,y)dxdy) &= \int_y^{y+dy} h(x,y)v(x,y)c(x,y)dy - \int_y^{y+dy} h(x,y)D(x,y)\frac{\partial c(x,y)}{\partial x}|_x dy \\ &- \int_x^{x+dx} h(x,y)D(x,y)\frac{\partial c(x,y)}{\partial y}|_y dx - \int_y^{y+dy} h(x+dx,y)v(x+dx,y)c(x+dx,y)dy \\ &- \int_y^{y+dy} h(x+dx,y)D(x+dx,y)\frac{\partial c(x,y)}{\partial x}|_{x+dx} dy - \int_x^{x+dx} h(x,y+dy)D(x,y+dy)\frac{\partial c(x,y)}{\partial y}|_{y+dy} dx \\ &+ (\text{predator-prey terms})h(x,y)dxdy\end{aligned}$$

Here c represents either phytoplankton P or zooplankton Z and the predator-prey terms are given by equations 2.3 and 2.4 respectively.

By applying the mean value theorem and lipschitz continuity to the equation the following is derived:

$$\begin{aligned}\frac{\partial}{\partial t}(h(x,y)c(x,y)dxdy) &= h(x,y)v(x,y)c(x,y)dy - h(x,y)D(x,y)\frac{\partial c(x,y)}{\partial x}|_x dy - h(x,y)D(x,y)\frac{\partial c(x,y)}{\partial y}|_y dx \\ &- h(x+dx,y)v(x+dx,y)c(x+dx,y)dy - h(x+dx,y)D(x+dx,y)\frac{\partial c(x,y)}{\partial x}|_{x+dx} dy \\ &- h(x,y+dy)D(x,y+dy)\frac{\partial c(x,y)}{\partial y}|_{y+dy} dx + (\text{predator-prey terms})h(x,y)dxdy\end{aligned}$$

As the volume $h(x,y)dxdy$ is independent of time, this factor can be taken in front of the time derivative. Furthermore, the equation is divided by $h(x,y)dxdy$ and reshuffled.

$$\begin{aligned}\frac{\partial c(x,y)}{\partial t} &= -\frac{1}{h(x,y)}\frac{h(x+dx,y)v(x+dx,y)c(x+dx,y) - h(x,y)v(x,y)c(x,y)}{dx} \\ &+ \frac{1}{h(x,y)}\frac{h(x+dx,y)D(x+dx,y)\frac{\partial c(x,y)}{\partial x}|_{x+dx} - h(x,y)D(x,y)\frac{\partial c(x,y)}{\partial x}|_x}{dx} \\ &+ \frac{1}{h(x,y)}\frac{h(x,y+dy)D(x,y+dy)\frac{\partial c(x,y)}{\partial y}|_{y+dy} - h(x,y)D(x,y)\frac{\partial c(x,y)}{\partial y}|_y}{dy} \\ &+ (\text{predator-prey terms})\end{aligned}$$

Now, the limits $dx \to 0$ and $dy \to 0$ are taken. Therefore, the equation can be rewritten with partial derivatives.

$$\frac{\partial c(x,y)}{\partial t} = -\frac{1}{h(x,y)}\frac{\partial}{\partial x}(h(x,y)v(x,y)c(x,y)) + \frac{1}{h(x,y)}\frac{\partial}{\partial x}(h(x,y)D(x,y)\frac{\partial c(x,y)}{\partial x}) + \frac{1}{h(x,y)}\frac{\partial}{\partial y}(h(x,y)D(x,y)\frac{\partial c(x,y)}{\partial y}) + \text{(predator-prey terms)}$$

The water flow is the same everywhere: $h(x,y)v(x,y) =$ constant. There are no places where the water can pile up or disappear. Therefore $h(x,y)v(x,y)$ can be taken in front of the x derivative, resulting in:

$$\frac{\partial c(x,y)}{\partial t} = -v(x,y)\frac{\partial c(x,y)}{\partial x} + \frac{1}{h(x,y)}\frac{\partial}{\partial x}(h(x,y)D(x,y)\frac{\partial c(x,y)}{\partial x}) + \frac{1}{h(x,y)}\frac{\partial}{\partial y}(h(x,y)D(x,y)\frac{\partial c(x,y)}{\partial y}) + \text{(predator-prey terms)} \tag{B.1}$$

Substituting $c = P$ and $c = Z$, the following system of equations is found:

$$\frac{\partial P(x,y)}{\partial t} = -v(x,y)\frac{\partial P(x,y)}{\partial x} + \frac{1}{h(x,y)}\frac{\partial}{\partial x}(h(x,y)D(x,y)\frac{\partial P(x,y)}{\partial x}) + \frac{1}{h(x,y)}\frac{\partial}{\partial y}(h(x,y)D(x,y)\frac{\partial P(x,y)}{\partial y}) + I(t)f(P) - Zg(P) \tag{B.2}$$

$$\frac{\partial Z(x,y)}{\partial t} = -v(x,y)\frac{\partial Z(x,y)}{\partial x} + \frac{1}{h(x,y)}\frac{\partial}{\partial x}(h(x,y)D(x,y)\frac{\partial Z(x,y)}{\partial x}) + \frac{1}{h(x,y)}\frac{\partial}{\partial y}(h(x,y)D(x,y)\frac{\partial Z(x,y)}{\partial y}) + \alpha g(P)Z - \alpha h(Z)Z \tag{B.3}$$

C

Computing the matrix and vectors of numerical approximation

In this appendix the derivation of the matrix **M** and the vectors **V** and **W** is given.

First of all, the functions $A_{n,m}$, $B_{n,m}$, $C_{n,m}$, $D_{n,m}$, $E_{n,m}$ can be subtracted from the equations derived in section 3.2.1. The other functions result from the boundary conditions.

From the boundary condition $c(0,m,t) = c_{left}$, for P it follows that $P_{0,m} = P_{left}$. Substituting this in the equation for $\frac{\partial P_{1,m}}{\partial t}$, the following equation can be formed:

$$\begin{aligned}\frac{\partial P_{1,m}}{\partial t} &= (\frac{h_{\frac{3}{2},m}D_{\frac{3}{2},m}}{h_{1,m}\Delta x^2})P_{2,m} + (\frac{h_{1,m+\frac{1}{2}}D_{1,m+\frac{1}{2}}}{h_{1,m}\Delta y^2})P_{1,m+1} \\ &+ (-\frac{h_{\frac{3}{2},m}D_{\frac{3}{2},m} + h_{\frac{1}{2},m}D_{\frac{1}{2},m}}{h_{1,m}\Delta x^2} - \frac{h_{1,m+\frac{1}{2}}D_{1,m+\frac{1}{2}} + h_{1,m-\frac{1}{2}}D_{1,m-\frac{1}{2}}}{h_{1,m}\Delta y^2} - \frac{v_{1,m}}{\Delta x})P_{1,m} \\ &+ (\frac{h_{\frac{1}{2},m}D_{\frac{1}{2},m}}{h_{1,m}\Delta x^2} + \frac{v_{1,m}}{\Delta x})P_{left} + (\frac{h_{1,m-\frac{1}{2}}D_{1,m-\frac{1}{2}}}{h_{1,m}\Delta y^2})P_{1,m-1} \\ &+ I(t)f(P_{1,m}) - Z_{1,m}g(P_{1,m})\end{aligned}$$

Thus in the matrix **M** in the row corresponding to $P_{0,m}$, the $D_{n,m}$ is left out, however in the vector **V**, $D_n^* P_{left}$ is added, where D_n^* equals the term $\frac{h_{\frac{1}{2},m}D_{\frac{1}{2},m}}{h_{1,m}\Delta x^2} + \frac{v_{1,m}}{\Delta x}$ subtracted from the above equation.

From the boundary condition $c(L,m,t) = c_{right}$, for P it follows that $P_{N_x+1,m} = P_{right}$. Substituting this in the equation for $\frac{\partial P_{N_x,m}}{\partial t}$, the following equation can be formed:

$$\begin{aligned}\frac{\partial P_{N_x,m}}{\partial t} &= (\frac{h_{N_x+\frac{1}{2},m}D_{N_x+\frac{1}{2},m}}{h_{N_x,m}\Delta x^2})P_{right} + (\frac{h_{N_x,m+\frac{1}{2}}D_{N_x,m+\frac{1}{2}}}{h_{N_x,m}\Delta y^2})P_{N_x,m+1} \\ &+ (-\frac{h_{N_x+\frac{1}{2},m}D_{N_x+\frac{1}{2},m} + h_{N_x-\frac{1}{2},m}D_{N_x-\frac{1}{2},m}}{h_{N_x,m}\Delta x^2} - \frac{h_{N_x,m+\frac{1}{2}}D_{N_x,m+\frac{1}{2}} + h_{N_x,m-\frac{1}{2}}D_{N_x,m-\frac{1}{2}}}{h_{N_x,m}\Delta y^2} - \frac{v_{N_x,m}}{\Delta x})P_{N_x,m} \\ &+ (\frac{h_{N_x-\frac{1}{2},m}D_{N_x-\frac{1}{2},m}}{h_{N_x,m}\Delta x^2} + \frac{v_{N_x,m}}{\Delta x})P_{N_x-1,m} + (\frac{h_{N_x,m-\frac{1}{2}}D_{N_x,m-\frac{1}{2}}}{h_{N_x,m}\Delta y^2})P_{N_x,m-1} \\ &+ I(t)f(P_{N_x,m}) - Z_{N_x,m}g(P_{N_x,m})\end{aligned}$$

Thus in the matrix **M** in the row corresponding to $P_{N_x,m}$, the $B_{n,m}$ is left out, however in the vector **V**, $B_n^* P_{right}$ is added, where B_n^* equals the term $\frac{h_{N_x+\frac{1}{2},m}D_{N_x+\frac{1}{2},m}}{h_{N_x,m}\Delta x^2}$ subtracted from the above equation.

From the boundary condition $c(x,H,t) = c_{ocean}$, for P it follows that $P_{n,N_y+1} = P_{ocean}$. Substituting this in the equation for $\frac{\partial P_{n,N_y}}{\partial t}$, the following equation can be formed:

$$\begin{aligned}\frac{\partial P_{n,N_y}}{\partial t} &= (\frac{h_{n+\frac{1}{2},N_y} D_{n+\frac{1}{2},N_y}}{h_{n,N_y}\Delta x^2}) P_{n+1,N_y} + (\frac{h_{n,N_y+\frac{1}{2}} D_{n,N_y+\frac{1}{2}}}{h_{n,N_y}\Delta y^2}) P_{ocean} \\ &+ (-\frac{h_{n+\frac{1}{2},N_y} D_{n+\frac{1}{2},N_y} + h_{n-\frac{1}{2},N_y} D_{n-\frac{1}{2},N_y}}{h_{n,N_y}\Delta x^2} - \frac{h_{n,N_y+\frac{1}{2}} D_{n,N_y+\frac{1}{2}} + h_{n,N_y-\frac{1}{2}} D_{n,N_y-\frac{1}{2}}}{h_{n,N_y}\Delta y^2} - \frac{v_{n,N_y}}{\Delta x}) P_{n,N_y} \\ &+ (\frac{h_{n-\frac{1}{2},N_y} D_{n-\frac{1}{2},N_y}}{h_{n,N_y}\Delta x^2} + \frac{v_{n,N_y}}{\Delta x}) P_{n-1,N_y} + (\frac{h_{n,N_y-\frac{1}{2}} D_{n,N_y-\frac{1}{2}}}{h_{n,N_y}\Delta y^2}) P_{n,N_y-1} \\ &+ I(t) f(P_{n,N_y}) - Z_{n,N_y} g(P_{n,N_y})\end{aligned}$$

Thus in the matrix $\mathbf{M}$ in the row corresponding to P_{n,N_y}, the $C_{n,m}$ is left out, however in the vector $\mathbf{V}$, $C_n^* P_{ocean}$ is added, where C_n^* equals the term $\frac{h_{n,N_y+\frac{1}{2}} D_{n,N_y+\frac{1}{2}}}{h_{n,N_y}\Delta y^2}$ subtracted from the above equation.

From the boundary condition $\frac{\partial c(x,0,t)}{\partial y} = 0$, for P it follows that $\frac{\partial P_{n,0}}{\partial y} = 0$. Using backward differentiation: $\frac{P_{n,0} - P_{n,-1}}{\Delta y} = 0$, giving $P_{n,-1} = P_{n,0}$. For $\frac{\partial P_{n,0}}{\partial t}$ this leads to the following equation:

$$\begin{aligned}\frac{\partial P_{n,N_y}}{\partial t} &= (\frac{h_{n+\frac{1}{2},0} D_{n+\frac{1}{2},0}}{h_{n,0}\Delta x^2}) P_{n+1,0} + (\frac{h_{n,\frac{1}{2}} D_{n,\frac{1}{2}}}{h_{n,0}\Delta y^2}) P_{n,1} \\ &+ (-\frac{h_{n+\frac{1}{2},0} D_{n+\frac{1}{2},0} + h_{n-\frac{1}{2},0} D_{n-\frac{1}{2},0}}{h_{n,0}\Delta x^2} - \frac{h_{n,\frac{1}{2}} D_{n,\frac{1}{2}} + h_{n,-\frac{1}{2}} D_{n,-\frac{1}{2}}}{h_{n,0}\Delta y^2} - \frac{v_{n,0}}{\Delta x}) P_{n,0} \\ &+ (\frac{h_{n-\frac{1}{2},0} D_{n-\frac{1}{2},0}}{h_{n,0}\Delta x^2} + \frac{v_{n,0}}{\Delta x}) P_{n-1,0} + (\frac{h_{n,-\frac{1}{2}} D_{n,-\frac{1}{2}}}{h_{n,0}\Delta y^2}) P_{n,0} \\ &+ I(t) f(P_{n,0}) - Z_{n,0} g(P_{n,0})\end{aligned}$$

Which can be rewritten to:

$$\begin{aligned}\frac{\partial P_{n,N_y}}{\partial t} &= (\frac{h_{n+\frac{1}{2},0} D_{n+\frac{1}{2},0}}{h_{n,0}\Delta x^2}) P_{n+1,0} + (\frac{h_{n,\frac{1}{2}} D_{n,\frac{1}{2}}}{h_{n,0}\Delta y^2}) P_{n,1} \\ &+ (-\frac{h_{n+\frac{1}{2},0} D_{n+\frac{1}{2},0} + h_{n-\frac{1}{2},0} D_{n-\frac{1}{2},0}}{h_{n,0}\Delta x^2} - \frac{h_{n,\frac{1}{2}} D_{n,\frac{1}{2}}}{h_{n,0}\Delta y^2} - \frac{v_{n,0}}{\Delta x}) P_{n,0} \\ &+ (\frac{h_{n-\frac{1}{2},0} D_{n-\frac{1}{2},0}}{h_{n,0}\Delta x^2} + \frac{v_{n,0}}{\Delta x}) P_{n-1,0} \\ &+ I(t) f(P_{n,0}) - Z_{n,0} g(P_{n,0})\end{aligned}$$

Therefore in the matrix $\mathbf{M}$ in the row corresponding to $P_{n,0}$, the $E_{n,m}$ is left out and $A_{n,m}$ is substituted by $A^*_{n,m}$ which equals the term $-\frac{h_{n+\frac{1}{2},0} D_{n+\frac{1}{2},0} + h_{n-\frac{1}{2},0} D_{n-\frac{1}{2},0}}{h_{n,0}\Delta x^2} - \frac{h_{n,\frac{1}{2}} D_{n,\frac{1}{2}}}{h_{n,0}\Delta y^2} - \frac{v_{n,0}}{\Delta x}$ subtracted from the above equation.

Here, all values are derived using P. For Z this derivation is exactly the same except that the boundary conditions are given by other values.

D

Code

In this appendix, the basis of the code is given. This consists of the code with which a time step in the formed numerical model can be computed and the code with which a solution for the 0D Steele and Henderson model can be computed, including its dependence of time. For other code, which consists essentially of analysis, one can email B.M.Vos@student.tudelft.nl.

D.1. Code for time step in 2D model

```
import numpy as np
import matplotlib.pyplot as plt
from scipy.sparse import spdiags
import scipy.sparse as sp

#define parameters Steele and Henderson (3 dagen)
It = 1
beta = 1
labda = 1
mu = 1
c = 10
alpha = 0.5
a = 0.5

#define parameters Diffusion and Convection
L = 500000 #m, 500 km
H = 5000 #m, 5 km
N_y = 80 #aantal gridpunten
N_x = 200
T = 5000 #aantal tijdstappen
dt = 20000 #s, grootte tijdstap

#changing depth
depth = np.array([])
depthy = np.linspace(5,50,N_y+2,endpoint=True)
for i in range(len(depthy)):
    depth = np.append(depth, depthy[i]*np.ones((N_x+2)))

# three terms: pp, conv, diff
roofdierprooiuitschakel = 1
v = 0*np.ones((N_x+2)*(N_y+2))
Diff = 10*np.ones((N_x+2)*(N_y+2))

#which model
n = 1
m = 1
```

```
37
38  #define initial condition
39  P_0 = 7*np.ones(N_x*(N_y+1))
40  Z_0 = 2.4*np.ones(N_x*(N_y+1))
41
42  #define boundary conditions
43  ### interchanged left and right boundary so that the v could be positive
44  P_n_H = 1.75
45  P_0_m = 8.75
46  P_L_m = 4.375
47
48  Z_n_H = 2.3
49  Z_0_m = 1.2
50  Z_L_m = 3
51
52  #define functions Steele and Henderson
53  def f(P):
54      return beta*P*(1-P/c)
55
56  def g(P,n):
57      return labda*P**n/(1+P**n)
58
59  def h(Z,m,a):
60      return a*Z**(m-1)
61
62  def dP(It,P,Z,n):
63      return roofdierprooiuitschakel*(It*f(P)-g(P,n)*Z)/3600/24/3
64
65  def dZ(P,Z,m,n,a):
66      return roofdierprooiuitschakel*(alpha*g(P,n)*Z - alpha*h(Z,m,a)*Z)/3600/24/3
67
68  # compute matrix M
69  dx = L/N_x
70  dy = H/N_y
71
72  #values at 1/2 grid
73  def vector_val(vector,n,m): #get wanted value from lexicographic vector
74      return vector[m*(N_x+2)+(n)]
75
76  def half(function,n,m,sign_n,sign_m): #get half value
77      (vector_val(function,(n+sign_n),(m+sign_m))+vector_val(function,n,m))/2
78      return (vector_val(function,(n+sign_n),(m+sign_m))+vector_val(function,n,m))/2
79
80  #define terms in matrix
81  def A(n,m):
82      return
            -(half(depth,n,m,+1,0)*half(Diff,n,m,+1,0)+half(depth,n,m,-1,0)*half(Diff,n,m,-1,0))/(vector_val(depth,n
            -(half(depth,n,m,0,+1)*half(Diff,n,m,0,+1)+half(depth,n,m,0,-1)*half(Diff,n,m,0,-1))/(vector_val(depth,n
            - (vector_val(v,n,m)/dx)
83
84  def B(n,m):
85      return (half(depth,n,m,+1,0)*half(Diff,n,m,+1,0))/(vector_val(depth,n,m)*dx**2)
86
87  def C(n,m):
88      return (half(depth,n,m,0,+1)*half(Diff,n,m,0,+1))/(vector_val(depth,n,m)*dy**2)
89
90  def D(n,m):
91      return (half(depth,n,m,-1,0)*half(Diff,n,m,-1,0))/(vector_val(depth,n,m)*dx**2) +
            vector_val(v,n,m)/dx
92
93  def E(n,m):
```

```
    return (half(depth,n,m,0,-1)*half(Diff,n,m,0,-1))/(vector_val(depth,n,m)*dy**2)

def A_bc(n):
    return
        -(half(depth,n,0,+1,0)*half(Diff,n,0,+1,0)+half(depth,n,0,-1,0)*half(Diff,n,0,-1,0))/(vector_val(depth,n
        -(half(depth,n,0,0,+1)*half(Diff,n,0,0,+1))/(vector_val(depth,n,0)*dy**2)
        -(vector_val(v,n,0)/dx)

def createM(N_x, N_y, depth, Diff, v, L, H):
    global A, B, C, D, E, A_bc

    ax_A = []
    ax_B = []
    ax_C = []
    ax_D = []
    ax_E = []

    ax_B.append(0)
    for i in range(N_x):
        ax_C.append(0)

    for m in range(0,N_y+1):
        for n in range(1,N_x+1):
            if m == 0:
                ax_A.append(A_bc(n))
                ax_C.append(C(n,m))
            elif m == N_y:
                ax_A.append(A(n,m))
                ax_E.append(E(n,m))
            else:
                ax_A.append(A(n,m))
                ax_C.append(C(n,m))
                ax_E.append(E(n,m))

            if n == 1:
                ax_B.append(B(n,m))
                ax_D.append(0)
            elif n == N_x:
                ax_B.append(0)
                ax_D.append(D(n,m))
            else:
                ax_B.append(B(n,m))
                ax_D.append(D(n,m))

    ax_D = ax_D[1:]
    ax_D.append(0)
    ax_B = ax_B[:-1]
    for i in range(N_x):
        ax_E.append(0)

    diags = np.array([-N_x,-1,0,1,N_x])
    M = spdiags([ax_E,ax_D,ax_A, ax_B, ax_C], diags, (N_x*(N_y+1)), (N_x*(N_y+1)))

    return M

#compute vector V and W

#vector V
def D_bc_P(m):
    return ((half(depth,1,m,-1,0)*half(Diff,1,m,-1,0))/(vector_val(depth,1,m)*dx**2) +
        vector_val(v,1,m)/dx)*P_0_m
```

```
151
152 def B_bc_P(m):
153     return
          ((half(depth,N_x,m,+1,0)*half(Diff,N_x,m,+1,0))/(vector_val(depth,N_x,m)*dx**2))*P_L_m
154
155 def C_bc_P(n):
156     return
          ((half(depth,n,N_y,0,+1)*half(Diff,n,N_y,0,+1))/(vector_val(depth,n,N_y)*dy**2))*P_n_H
157
158 def createV(N_x, N_y):
159     V = np.zeros(N_x*(N_y+1))
160     for i in range(1,N_x+1):
161         for j in range(0,N_y+1):
162             if i == 1 and j == N_y:
163                 V[j*(N_x)+(i-1)] = D_bc_P(m) + C_bc_P(n)
164             elif i == N_x and j == N_y:
165                 V[j*(N_x)+(i-1)] = B_bc_P(m) + C_bc_P(n)
166             elif i == 1:
167                 V[j*(N_x)+(i-1)] = D_bc_P(m)
168             elif i == N_x:
169                 V[j*(N_x)+(i-1)] = B_bc_P(m)
170             elif j == N_y:
171                 V[j*(N_x)+(i-1)] = C_bc_P(n)
172     return V
173
174 # vector W
175 def D_bc_Z(m):
176     return ((half(depth,1,m,-1,0)*half(Diff,1,m,-1,0))/(vector_val(depth,1,m)*dx**2) +
          vector_val(v,1,m)/dx)*Z_0_m
177
178 def B_bc_Z(m):
179     return
          ((half(depth,N_x,m,+1,0)*half(Diff,N_x,m,+1,0))/(vector_val(depth,N_x,m)*dx**2))*Z_L_m
180
181 def C_bc_Z(n):
182     return
          ((half(depth,n,N_y,0,+1)*half(Diff,n,N_y,0,+1))/(vector_val(depth,n,N_y)*dy**2))*Z_n_H
183
184 def createW(N_x, N_y):
185     W = np.zeros(N_x*(N_y+1))
186     for i in range(1,N_x+1):
187         for j in range(0,N_y+1):
188             if i == 1 and j == N_y:
189                 W[j*(N_x)+(i-1)] = D_bc_Z(m) + C_bc_Z(n)
190             elif i == N_x and j == N_y:
191                 W[j*(N_x)+(i-1)] = B_bc_Z(m) + C_bc_Z(n)
192             elif i == 1:
193                 W[j*(N_x)+(i-1)] = D_bc_Z(m)
194             elif i == N_x:
195                 W[j*(N_x)+(i-1)] = B_bc_Z(m)
196             elif j == N_y:
197                 W[j*(N_x)+(i-1)] = C_bc_Z(n)
198     return W
199
200 M = createM(N_x, N_y, depth, D, v, L, H)
201 V = createV(N_x, N_y)
202 W = createW(N_x, N_y)
203 I = sp.eye(N_x*(N_y+1))
204
205 def solve_SP_thread(A, b):
206     return sp.linalg.spsolve(A,b)
```

```
207
208 def timestep(dt,P,Z,M,V,W):
209     with concurrent.futures.ThreadPoolExecutor() as executor:
210         future1 = executor.submit(solve_SP_thread, (I-dt*M), (P+dt*(V+dP(It,P,Z,n))))
211         future2 = executor.submit(solve_SP_thread, (I-dt*M), (Z+dt*(W+dZ(P,Z,m,n,a))))
212         p_next = future1.result()
213         z_next = future2.result()
214         return p_next,z_next
```

D.2. Code for model run 0D model

```
1  def mu_Eppley(T):
2      mu = 10**(0.0275*T - 0.07)
3      return mu
4
5  P = np.linspace(0,10,100,endpoint = True)
6  def f(P,T):
7      f = 3*mu_Eppley(T)*P*(1-P/c) #temperature dependence
8      #f=P*(1-P/c)
9      return f
10
11 def g(P,n):
12     g=(lamda*P**n)/(1+P**n)
13     return g
14
15 def h(Z,m,a):
16     h= a*Z**(m-1)
17     return h
18
19 def I(t):
20     I = 1 + 0.5*np.sin(t*2*np.pi/100)
21     return I
22
23 def run_model(a,m,n,P0,Z0,dt):
24     t_fin=600
25     dt3days = dt/(3600*24*3)
26     t = []
27     i = 0
28     t.append(i)
29     while i<t_fin:
30         i += dt3days
31         t.append(i)
32
33     p=P0
34     z=Z0
35     P=[p]
36     Z=[z]
37     for i in range(1,len(t)):
38         dPdt=f(p,T)-z*g(p,n)
39         dZdt= alpha*g(p,n)*z - alpha*h(z,m,a)*z
40         p += dPdt*dt3days
41         z += dZdt*dt3days
42         P.append(p)
43         Z.append(z)
44
45     peaks, _ = sig.find_peaks(Z)
46     if len(peaks)>1:
47         period = 3*(t[peaks[-1]]-t[peaks[-2]])
48     else:
```

```
        period =0

    fig, axs = plt.subplots(2, 1)
    axs[0].plot(3*np.array(t), P, label = '$P$')
    axs[1].plot(3*np.array(t), Z, label = '$Z$')
    axs[0].set_ylabel('P (mg/m$^3$)')
    axs[1].set_ylabel('Z (mg/m$^3$)')
    axs[1].set_xlabel('Time (days)')

    for ax in fig.get_axes():
        ax.label_outer()

    return period
```

E

Analytical solutions convection and diffusion

To validate the created model, it is necessary to compare some results of the model to an analytical solution. Of some extreme such an analytical solution can be derived. These derivation are given in this chapter.

E.1. Analytical solution 1D convection

The first situation that can be tested is the situation where only convection is allowed, resulting in the following equation:

$$\frac{\partial P}{\partial t} = -v\frac{\partial P}{\partial x} \tag{E.1}$$

This equation only has one boundary condition $P(0,t) = P_{left}$ and and an initial condition $P(x,0) = P_i$. The problem has the following solution:

$$P(x,t) = \begin{cases} P_{left} & \text{if } x \leq vt \\ P_i & \text{if } x > vt \end{cases} \tag{E.2}$$

E.2. Analytical solution 1D diffusion

The 1D diffusion problem is given by the following equation:

$$\frac{\partial P}{\partial t} = D\frac{\partial^2 P}{\partial y^2}, \tag{E.3}$$

with $P(0,t) = P_{ocean}$, $P(2H,t) = P_{ocean}$ and $P(y,0) = P_i$. Note that the domain is mirrored in the y-direction to get rid of the Neumann boundary condition $\frac{\partial P(x,t)}{\partial y} = 0$ and shifted to begin at $y = 0$. To determine the solution of this problem the solution is split in a steady state solution with non homogeneous boundary conditions and a homogeneous solution.

The problem corresponding to steady state is:

$$\frac{\partial^2 P_E}{\partial x^2} = 0, \qquad P_E(0) = P_{ocean}, \qquad P_E(2H) = P_{ocean} \tag{E.4}$$

This problem has the solution:

$$P_E(x) = P_{ocean} \tag{E.5}$$

Now using that $v(x,t) = P(x,t) - P_E(x)$, the homogeneous problem is:

$$\frac{\partial v}{\partial t} = D\frac{\partial^2 v}{\partial x^2}, \qquad v(0,t) = 0, \qquad v(2H,t) = 0, \qquad v(x,0) = P_i - P_E(x) \tag{E.6}$$

Which has the following solution:

$$\begin{aligned} v(x,t) &= \textstyle\sum_{n=1}^{\infty} a_n sin(\frac{n\pi x}{2H}) e^{-k(\frac{n\pi}{2H})^2 t} \\ a_n &= \tfrac{1}{H}\textstyle\int_0^{2H} [P_i - P_{ocean}] sin(\frac{n\pi x}{2H}) dx \end{aligned} \tag{E.7}$$

Together these two solutions form the solution to the 1D diffusion problem: $P(x,t) = P_E(x) + v(x,t)$. Thus:

$$P(x,t) = P_{ocean} \sum_{n=1}^{\infty} a_n sin(\frac{n\pi x}{2H}) e^{-k(\frac{n\pi}{2H})^2 t} \tag{E.8}$$

E.3. Analytical solution 2D diffusion

The 2D diffusion problem is given by:

$$\frac{\partial P}{\partial t} = D\frac{\partial^2 P}{\partial x^2} + D\frac{\partial^2 P}{\partial y^2}, \tag{E.9}$$

with $P(0,y,t) = P_{left}$, $P(L,y,t) = P_{right}$, $P(x,H,t) = P_{ocean}$, $\frac{\partial P(x,0,t)}{\partial y} = 0$ and $P(x,0) = P_i$. The Neumann boundary condition makes the problem harder to solve analytically. To avoid this, symmetry is used: underneath a mirrored region in the x axis is added and the region is shifted to start at the x axis, as depicted in figure E.1.

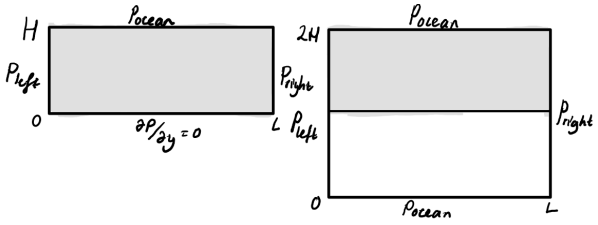

Figure E.1

Now the boundary conditions in the y-direction are $P(x,2H,t) = P_{ocean}$ and $P(x,0,t) = P_{ocean}$. The other conditions remain the same.

The method to solve this problem is the same as for the 1D diffusion problem: the solution is split in a steady state solution with non homogeneous boundary conditions and a homogeneous solution.

The steady state problem is split into four separate problems [9], which all only have one boundary condition not equal to zero, as depicted in figure E.2.

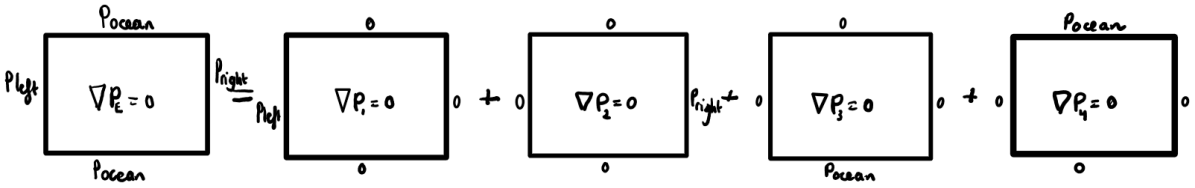

Figure E.2

$$P_E(x,y) = P_1(x,y) + P_2(x,y) + P_3(x,y) + P_4(x,y) \tag{E.10}$$

To demonstrate how these solutions are derived, the steps of the derivation of $P_1(x,y)$ is written down. The problem is:

$$\frac{\partial^2 P_1}{\partial x^2} + \frac{\partial^2 P_1}{\partial y^2} = 0, \tag{E.11}$$

with $P_1(0,y) = P_{left}$, $P_1(L,y) = 0$, $P_1(x,0) = 0$, $P_1(x,2H) = 0$.

First of all, separation of variables is applied to the solution: $P_1(x,y) = X(x)Y(y)$, which results in the following equations:

$$\begin{aligned} X"(x) - \lambda X(x) = 0 \\ Y"(y) + \lambda Y(y) = 0 \end{aligned} \tag{E.12}$$

These equations have boundary conditions $X(L) = 0$, $Y(0) = 0$ and $Y(2H) = 0$. There solutions are given by:

$$\begin{aligned} Y_n(y) &= sin(\tfrac{n\pi y}{2H}), \qquad \lambda_n = (\tfrac{n\pi}{2H})^2 \\ X_n(x) &= c_1 cosh(\tfrac{n\pi(x-L)}{2H}) + c_2 sinh(\tfrac{n\pi(x-L)}{2H}) \end{aligned} \tag{E.13}$$

By the boundary condition $X(L) = 0$, $c_1 = 0$. Thus $X_n(x) = c_2 sinh(\frac{n\pi(x-L)}{2H})$. The solution thus is:

$$P_1(x,y) = \sum_{n=1}^{\infty} A_n sinh(\frac{n\pi(x-L)}{2H}) sin(\frac{n\pi y}{2H}) \tag{E.14}$$

Here A_n can be found using the non homogeneous boundary condition $P_1(x,0) = P_{left}$. Then, it follows that

$$A_n = \frac{2}{2H sin(\frac{-n\pi L}{2H})} \int_0^{2H} P_{left} sin(\frac{n\pi y}{2H}) dy \tag{E.15}$$

The same way $P_2(x,y)$, $P_3(x,y)$ and $P_4(x,y)$ can be derived, resulting in:

$$\begin{aligned} P_2(x,y) &= \textstyle\sum_{n=1}^{\infty} B_n sinh(\frac{n\pi x}{2H}) sin(\frac{n\pi y}{2H}) \\ B_n &= \frac{2}{2H sin(\frac{n\pi L}{2H})} \int_0^{2H} P_{right} sin(\frac{n\pi y}{2H}) dy \end{aligned} \tag{E.16}$$

$$\begin{aligned} P_3(x,y) &= \textstyle\sum_{n=1}^{\infty} C_n sinh(\frac{n\pi(y-2H)}{L}) sin(\frac{n\pi x}{L}) \\ C_n &= \frac{2}{L sin(\frac{-2n\pi H}{L})} \int_0^{L} P_{ocean} sin(\frac{n\pi x}{L}) dx \end{aligned} \tag{E.17}$$

$$\begin{aligned} P_4(x,y) &= \textstyle\sum_{n=1}^{\infty} D_n sinh(\frac{n\pi(y)}{L}) sin(\frac{n\pi x}{L}) \\ D_n &= \frac{2}{L sin(\frac{2n\pi H}{L})} \int_0^{L} P_{ocean} sin(\frac{n\pi x}{L}) dx \end{aligned} \tag{E.18}$$

Next, the homogeneous problem is solved, where $v(x,y,t) = P(x,y,t) - P_E(x,y)$ The problem is:

$$\frac{\partial v}{\partial t} = D\frac{\partial^2 v}{\partial x^2} + D\frac{\partial^2 v}{\partial y^2} \tag{E.19}$$

with $v(0,y,t) = 0$, $v(L,y,t) = 0$, $v(x,0,t) = 0$, $v(x,2H,t) = 0$ and $P(x,0) = P_i - P_E(x,y)$.
Using separation of variables, v(x,y,t) = X(x)Y(y)T(t), the following solution is derived [8]:

$$\begin{aligned} v(x,y,t) &= \textstyle\sum_{n=1}^{\infty} sum_{m=1}^{\infty} E_{mn} sin(\frac{n\pi x}{L}) sin(\frac{m\pi y}{2H}) e^{-\lambda_{mn}^2 t} \\ E_{mn} &= \tfrac{2}{HL} \textstyle\int_0^{L} \int_0^{2H} [P_i - P_E(x,y)] sin(\frac{n\pi x}{L}) sin(\frac{m\pi y}{2H}) dy dx \\ \lambda_{mn} &= \sqrt{D}\sqrt{(\tfrac{n\pi}{L})^2 + (\tfrac{m\pi}{2H})^2} \end{aligned} \tag{E.20}$$

Together these two solutions form the solution to the 2D diffusion problem: $P(x,y,t) = P_E(x,y) + v(x,y,t)$.

E.4. Analytical solution 1D diffusion and convection

The 1D problem with diffusion and convection is given by:

$$\frac{\partial P}{\partial t} = -v\frac{\partial P}{\partial x} + D\frac{\partial^2 P}{\partial x^2} \tag{E.21}$$

This problem can be solved analytically with the following boundary conditions and initial condition: $P(0,t) = P_{left}$, $P(\infty,t) = P_i$ and $P(x,0) = P_i$.

The solution to this problem is [14]:

$$P(x,t) = P_i + \frac{P_{left} - P_i}{2} (erfc(\frac{x - vt}{2\sqrt{Dt}}) + e^{\frac{vx}{D}} erfc(\frac{x+vt}{2\sqrt{Dt}})) \tag{E.22}$$

F

Visualisation effect diffusion and convection

To give some insight on the effect of the diffusion, convection and predator-prey model on the 2D model, in this appendix some plots are showed to visualize the effect.

F.1. Diffusion and predator-prey

The effect of diffusion on the predator-prey model is that it suppresses the limit cycle of the predator-prey model. This is shown in figure F.1 for $D = 1$ m^2/s. The further off the coast, the more the limit cycle is muted.

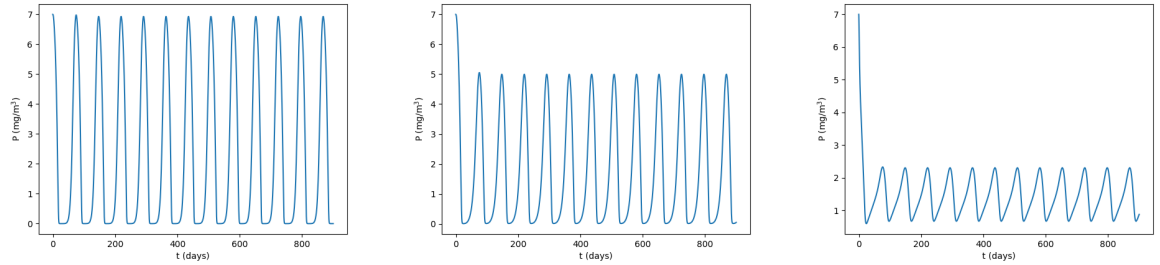

(a) Phytoplankton over time. $D = 1$ m^2/s, $x = 625$ m, $y = 250$ km.

(b) Phytoplankton over time. $D = 1$ m^2/s, $x = 2500$ m, $y = 250$ km.

(c) Phytoplankton over time. $D = 1$ m^2/s, $x = 4375$ m, $y = 250$ km.

Figure F.1

F.2. Convection and predator-prey

The effect of convection on the predator-prey model is that the limit cycle corresponding to the left boundary condition develops in the x-direction. Resulting in a steady state solution on each point. Before the left boundary condition reaches a point, the limit cycle corresponding to the initial condition occurs. This can be seen in figure F.2 for $v = 0.01$ m/s. The further from the left boundary, the longer the limit cycle corresponding to the initial condition is observed, before the point reaches steady state.

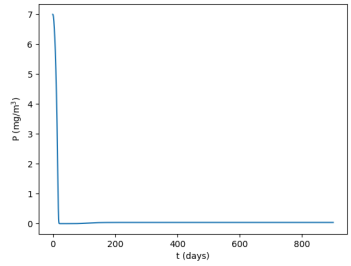

(a) Phytoplankton over time. $v = 0.01$ m/s, $x = 2.5$ km, $y = 50$ km.

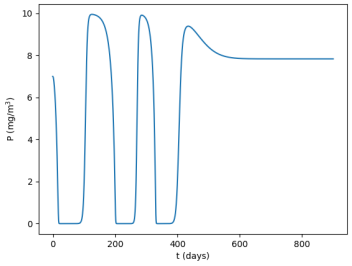

(b) Phytoplankton over time. $v = 0.01$ m/s, $x = 2.5$ km, $y = 250$ km.

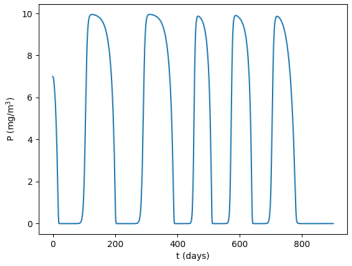

(c) Phytoplankton over time. $v = 0.01$ m/s, $x = 2.5$ km, $y = 450$ km.

Figure F.2

The higher the velocity, the less time the predator-prey model has to work on the left boundary condition before it reaches the end of the domain. Thus there are less fluctuations in the x-direction. This is displayed in figure F.3.

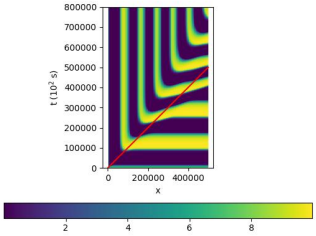

(a) Color coded solution of P over x and t for $v = 0.01$ m/s. In red the characteristic line corresponding to $v = 0.01$ m/s.

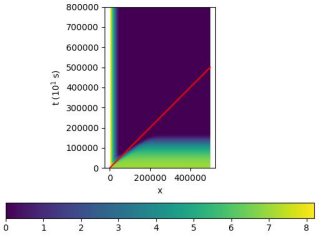

(b) Color coded solution of P over x and t for $v = 0.1$ m/s. In red the characteristic line corresponding to $v = 0.1$ m/s.

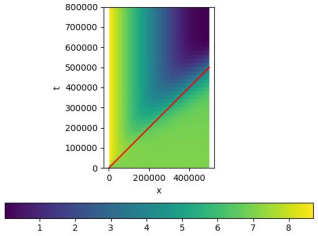

(c) Color coded solution of P over x and t for $v = 1$ m/s. In red the characteristic line corresponding to $v = 1$ m/s.

Figure F.3

F.3. Convection, diffusion and predator-prey

The effect of diffusion and convection is visualized in figure F.4. Here it can be seen that the effect of diffusion and convection separately are visible.

To visualize this effect of diffusion and convection the maximum and minimum value of P are plotted over x and y in figure F.5 for a period of time when the solution has converged to its equilibrium solution. In figure F.5a the oscillations in the x-directions are visible. In figure F.5 the diffusion in the y-direction is visible.

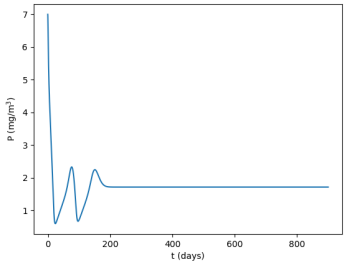

(a) Phytoplankton over time. $v = 0.02$ m/s, $D = 1$ m^2/s, $x = 4.375$ km, $y = 250$ km.

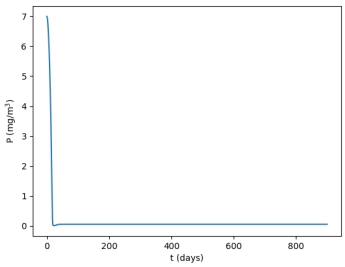

(b) Phytoplankton over time. $v = 0.02$ m/s, $D = 1$ m^2/s, $x = 2.5$ km, $y = 50$ km.

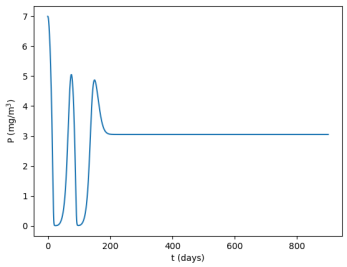

(c) Phytoplankton over time. $v = 0.02$ m/s, $D = 1$ m^2/s, $x = 2.5$ km, $y = 250$ km.

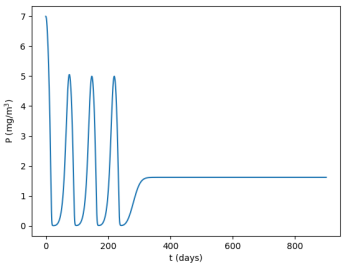

(d) Phytoplankton over time. $v = 0.02$ m/s, $D = 1$ m^2/s, $x = 2.5$ km, $y = 450$ km.

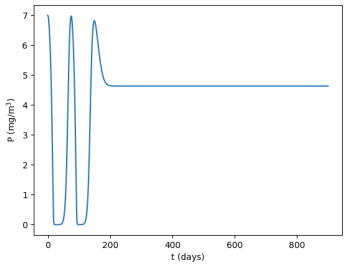

(e) Phytoplankton over time. $v = 0.02$ m/s, $D = 1$ m^2/s, $x = 0.625$ km, $y = 250$ km.

Figure F.4

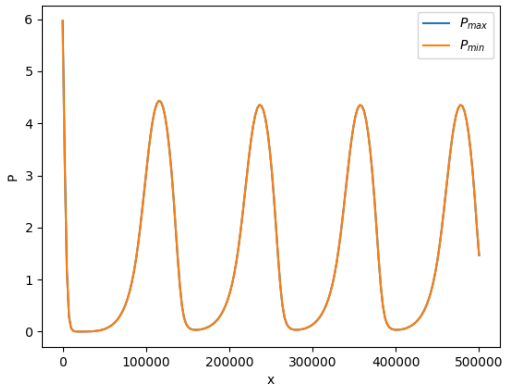

(a) Maximum and minimum of P (mg/m^3) over x (m) at y = 2.5 km for $v = 0.02$ m/s and $D = 1$ m^2/s.

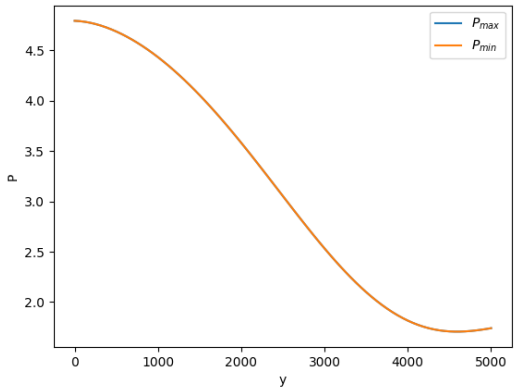

(b) Maximum and minimum of P (mg/m^3) over y (m) at x = 250 km for $v = 0.02$ m/s and $D = 1$ m^2/s.

Figure F.5